Pharmacology & Biomolecular Research (PBR)

HENDUN RESEARCH ACCESS

Research Article

An in Silico Annotated Drug Discovery Interactive Approach for The Depletion of Tumor-Associated Macrophages by A Computer-Aided Designed Canditate Druggable Toll-Like Receptor (Pam2IDG) Peptide-Domain Targeted by A Pharmacophoric Mimetic Agonistic Agent

Grigoriadis Ioannis[1*], Grigoriadis George[2]

[1] Department of Computer Drug Discovery Science, BiogenetoligandorolTM, Thessaloniki, Greece

[2] Department of Stem Cell Bank and ViroGeneaTM, Biogenea Pharmaceuticals Ltd, Thessaloniki, Greece

Abstract

It has been previosuly reported that lipopeptides can be used to elicit cytotoxic T lymphocyte (CTL) responses against viral diseases and cancer. In previous scientific projects, it has also been determined that mono- palmitoylated peptides can enhance anti-tumor responses in the absence of adjuvant activity. To investigate whether di- palmitoylated peptides with TLR2 agonist activity are able to induce anti-tumor immunity, it was previously synthesized a di-palmitic acid-conjugated long peptide that contains a murine CTL epitope of HPV E749-57 (Pam2IDG). Mathematical modeling and computer simulation have become crucial to biological fields from genomics to ecology. However, multi-cell, tissue-level simulations of development and disease have lagged behind other areas because they are mathematically more complex and lack easy-to-use software tools that allow building and running in- silico experiments without requiring in-depth knowledge of programming. As aresult we discovered for the first time, a Toll-like receptor agonist-conjugated peptide-mimetic pharmacophoric multi-targeted agent utilizing admetSAR: a comprehensive source and free tool for assessment of chemical ADMET properties based on a GRID-based three- dimensional pharmacophore on KLAPpharm within a novel KNIME-RDkit-CDK chemicalinformatic approach for conserved pharmacophore elucidation via a data mining analysis.

Keywords: *Toll-like receptor, agonist-conjugated, peptide-mimetic, pharmacophoric multi-targeted, mitosis, cell growth, cell sorting, chemotaxis, CPM, multi-cell modeling, tissue-level modeling, developmental biology, computational*

Introduction

Toll-like receptor (TLR) agonists beneficially modulate allergic airway inflammation. However, the efficiency of TLR agonists varies considerably, and their exact cellular mechanisms (especially of TLR 2/6 agonists) are incompletely understood. It has also been investigated at a cellular level whether the administration of the pharmacologically improved TLR2/6 agonist S-[2,3-bispalmitoyiloxy-(2R)-propyl]-R-cysteinyl- amido-monomethoxy polyethylene glycol (BPP) conjugated to antigenic peptide (BPP- OVA) could divert an existing Th2 response and influence airway eosinophilia. The effects of BPP-OVA on airway inflammation were assessed in a classic murine sensitization/challenge model and an adoptive transfer model, which involved the adoptive transfer of in vitro differentiated ovalbumin (OVA)–specific Th2 cells. Functional T-cell stimulation by lung dendritic cells (DCs) was determined both in vitro and in vivo, combined with a cytokine secretion analysis. A single mucosal application of BPP-OVA efficiently delivered antigen, led to TLR2-mediated DC activation, and resulted in OVA-specific T-cell proliferation via lung DCs in vivo. In alternative models of allergic airway disease, a single administration of BPP-OVA before OVA challenge (but not BPP alone) significantly reduced airway eosinophilia, most likely through altered antigen-specific T-cell stimulation via DCs. Analyses of adoptively transferred Th2-biased cells after BPP-OVA administration in vivo suggested that BPP-OVA guides antigen-specific Th2 cells to produce significantly higher amounts of IFN-γ upon allergen challenge. These data show for the first time that a single mucosal administration of a TLR 2/6 agonist–allergen conjugate can provoke IFN-γ responses in Th2-biased cells and alleviate allergic airway inflammation [8] contemporary life scientists, whether theoretical or experimental, have relatively narrow disciplinary training and specialization which is partly a consequence of the speed of current progress in the life sciences and concomitant growth in the number of active researchers. High-affinity antibodies are generated in germinal centers in a process involving mutation and selection of B cells. Information processing in germinal center reactions has been investigated in a number of recent experiments. These have revealed cell migration patterns, asymmetric cell divisions, and cell-cell interaction characteristics, used here to develop a theory of germinal center B cell selection, division, and exit (the LEDA model). According to this model, B cells selected by T follicular helper cells on the basis of successful antigen processing always return to the dark zone for asymmetric division, and acquired antigen is inherited

Corresponding author: Grigoriadis Ioannis, Department of Computer Drug Discovery Science, BiogenetoligandorolTM, Thessaloniki, Greece, Tel: +90 312 290 18 56; Fax: +90 312 290 18 56; E-mail: biogeneadrug@gmail.com**Received:** November 02 2016;

Received: October 21, 2016; **Accepted:** October 21, 2017; **Published:** December 21, 2017.

by one daughter cell only. Antigen- retaining B cells differentiate to plasma cells and leave the germinal center through the dark zone. This theory has implications for the functioning of germinal centers because compared to previous models, high-affinity antibodies appear one day earlier and the amount of derived plasma cells is considerably larger [91]. It has been reported that lipopeptides can be used to elicit cytotoxic T lymphocyte (CTL) responses against viral diseases and cancer. In our previous study, we determined that mono-palmitoylated peptides can enhance anti-tumor responses in the absence of adjuvant activity. To investigate whether di-palmitoylated peptides with TLR2 agonist activity are able to induce anti-tumor immunity, we synthesized a di-palmitic acid- conjugated long peptide that contains a murine CTL epitope of HPV E749–57 (Pam2IDG). Pam2IDG stimulated the maturation of bone marrow-derived dendritic cells (BMDCs) through TLR2/6. After immunization, Pam2IDG induced higher levels of T cell responses than those obtained with its non- lapidated counterpart (IDG). In the prophylactic model, Pam2IDG immunization completely inhibited tumor growth, whereas IDG immunization was unable to inhibit tumor growth. However, Pam2IDG immunization could not effectively inhibit the growth of established tumors. Therefore, it has been further investigated whether the depletion of immunosuppressive factors could improve the therapeutic effects of Pam2IDG. More data have been indicated that treatment with Pam2IDG combined with clodronate/liposome delays tumor growth and increases the survival rate. It has also been observed that the therapeutic effects of Pam2IDG are improved by diminishing the function of tumor-associate macrophages (TAMs) and through the use of an IL10 receptor blocking antibody or a Cyclooxygenase 2 (Cox-2) inhibitor. The depletion of TAMs may enhance the anti-tumor immunity of a TLR2 agonist-conjugated peptide [30]. Protein-protein and protein- ligand interactions are ubiquitous in a biological cell. Other inspected evidence have shown that a representative set of 1,611 representative protein-protein complexes and identified pockets with a potential for binding small molecule ligands. The majority of these pockets are within a 6 Å distance from protein interfaces. Accordingly, in about half of ligand-bound protein-protein complexes, amino acids from both sides of a protein interface are involved in direct contacts with at least one ligand. Statistically, ligands are closer to a protein-protein interface than a random surface patch of the same solvent accessible surface area. Similar results are obtained in an analysis of the ligand distribution around domain-domain interfaces of 1,416 nonredundant, two-domain protein structures. Furthermore, comparable sized pockets as observed in experimental structures are present in artificially generated protein complexes, suggesting that the prominent appearance of pockets around protein interfaces is mainly a structural consequence of protein packing and thus, is an intrinsic geometric feature of protein structure. Nature may take advantage of such a structural feature by selecting and further optimizing for biological function indicating that packing nearby protein-protein or domain- domain interfaces is a major route to the formation of ligand-binding pockets [64]. Computer simulation and associated experimental validation of assembly of glial- like support cells into the interweaving hexagonal lattice that spans the Drosophila pupal eye. This process of cell movements organizes the ommatidial array into a functional pattern. Unlike earlier simulations that focused on the arrangements of cells within individual ommatidia, here we examine the local movements that lead to large-scale organization of the emerging eye field. Simulations based on our experimental observations of cell adhesion, cell death, and cell movement successfully patterned a tracing of an emerging wild-type pupal eye. Surprisingly, altering cell adhesion had only a mild effect on patterning, contradicting our previous hypothesis that the patterning was primarily the result of preferential adhesion between IRM-class surface proteins. Instead, simulations highlighted the importance of programmed cell death (PCD) as well as a previously unappreciated variable: the expansion of cells' apical surface areas, which promoted rearrangement of neighboring cells. Prediction were also tested experimentally by preventing expansion in the apical area of individual cells: patterning was disrupted in a manner predicted by our simulations. More work has also been demonstrated the value of combining computer simulation with in vivo experiments to uncover novel mechanisms that are perpetuated throughout the eye field. It also demonstrates the utility of the Glazier–Graner– Hogeweg model (GGH) for modeling the links between local cellular interactions and emergent properties of developing epithelia as well as predicting unanticipated results in vivo [151]. While the success of contemporary biology might lead naïve observers to conclude that our understanding is a simple superposition of achievements in the subfields composing life sciences, only rarely can we understand how a biological phenomenon operates by analyzing and understanding how its isolated components operate. Just as knowing how transistors work is not sufficient to design and build a modern microprocessor, knowing the ‒function‖ of an enzyme does not suffice to design cells' biochemical networks or even to predict the phenotypic simulated effect of knocking out specific genes. *Systems biology* is a scientific discipline that studies complex interactions in biology, relying more on knowledge integration than on detailed studies of individual biological subsystems where systems biologists often build mathematical models and computer simulations of living cells, tissues, organs or even entire organisms to embody their understanding of this integration. The last decade has seen fairly realistic simulations of single cells that can confirm or predict experimental findings because they are computationally expensive, they can simulate at most several cells at even more detailed subcellular simulations can replicate some of the processes taking place inside individual cells. *E.g.*, Virtual Cell (http://www.nrcam.uchc.edu) supports microscopic simulations of intracellular dynamics to produce detailed replicas of individual cells, but can only simulate single cells or small cell clusters. Simulations of tissues, organs and organisms present a somewhat different challenge: how to simplify and adapt single cell simulations to apply them efficiently to study, *in-silico*, ensembles of several million cells to be useful, these simplified simulations should capture key cell- level behaviors, providing a phenomenological description of cell interactions without requiring prohibitively detailed molecular- level simulations of the internal state of each cell while an understanding of cell biology, biochemistry, genetics, *etc.* is essential for building useful, predictive simulations, the hardest part of simulation building is identifying and quantitatively describing appropriate subsets of this knowledge in the excitement of discovery, scientists often forget that modeling and simulation, by definition, require simplification of reality. One choice is to ignore cells completely, *e.g.*, Physiome [1] models tissues as continua with bulk mechanical properties and detailed molecular reaction networks, which is computationally efficient for describing dense tissues and non- cellular materials like bone, extracellular matrix (*ECM*), fluids, and diffusing chemicals [2,3], but not for situations where cells reorganize or migrate using multi-cell simulations that are useful to interpolate between single-cell and continuum-tissue extremes because cells provide a natural level of abstraction for simulation of tissues, organs and organisms [4]. Treating cells phenomenologically reduces the millions of interactions of gene products to several behaviors: most cells can move, divide, die, differentiate, change shape, exert forces, secrete and absorb chemicals and electrical charges, and change their distribution of surface properties where the *Glazier-Graner- Hogeweg*(*GGH*) approach facilitates multiscale simulations by defining spatially- extended *generalized cells*, which can represent clusters of cells, single cells, sub- compartments of single cells or small subdomains of non-cellular materials. This flexible definition allows tuning of the level of detail

in a simulation from intracellular to continuum without switching simulation framework to examine the simulated effect of changing the level of detail on a macroscopic outcome, *e.g.*, by switching from a coupled ordinary-differential-equation(*ODE*) *Reaction-Kinetics*(*RK*) model of gene regulation to a Boolean description or from a simulation that includes subcellular structures to one that neglects them on a Pam2IDG stimulation for the maturation of bone marrow-derived dendritic cells (BMDCs) through TLR2/6 where the immunization simulated logical system implemented to a logical system with the Pam2IDG induced higher levels of T cell responses than those obtained with its non-lapidated counterpart (IDG) [5]. The PBE combines the continuum electrostatics description of fixed charges in a dielectric medium with the Boltzmann prescription for mobile ions in aqueous solvent at the thermal equilibrium with a reservoir [12]. In its linearized form, which is valid for low ionic concentrations, the PBE rea$\nabla\cdot[\epsilon(x)\nabla\Phi(x)]+\rho fixed\epsilon 0=\epsilon solv\lambda 2\Phi(x)$ based on the –definition of synergy‖ which is one of the most confusing areas in biomedical sciences since there are about twenty different definitions for synergy in literature, but none supports the others [6,25,26]. equations with the presence and absence of an inhibitor, the common parameters such as K_m, K_i, and V_{max} can be cancelled out and yield the general equation for the dose and simulated effect [7,9,10]. Thus, for a two drug combination, in a first- order system (m=1), we get the general equation [11,12] on drug combination, which intends to obtain synergistic simulated effect or reduce toxicity, is of primary importance in treatments of the most dreadful diseases, such as cancer and AIDS [6,24]. Thus, the establishment of multiple drug combination is as important as a new drug development it has been reported that lipopeptides can be used to elicit cytotoxic T lymphocyte (CTL) responses against viral diseases and cancer. After immunization sikmulated logical system sikmulated logical system with the Pam2IDG it has been showed induction of higher levels of T cell responses than those obtained with its non-lipidated counterpart (IDG). In the prophylactic model, Pam2IDG immunization simulated logical system sikmulated logical system completely inhibited tumor growth, whereas IDG immunization sikmulated logical system sikmulated logical system was unable to inhibit tumor growth where Pam2IDG immunization sikmulated logical system sikmulated logical system could not simulated effectively inhibit the growth of established tumors. Therefore, we further investigated whether the depletion of immunosuppressive factors could improve the therapeutic simulated effects of Pam2IDG. Our data indicate that treatment with Pam2IDG combined with computer-aided designed neoligand456431/liposome delays tumor growth and increases the survival rate. We also observed that the therapeutic simulated effects of Pam2IDG are improved by diminishing the function of tumor-associate macrophages (TAMs) and through the use of an IL10 receptor blocking antibody or a Cyclooxygenase 2 (Cox-2) inhibitor [13-16]. In conclusion, the depletion of TAMs may enhance the anti-tumor immunity of a TLR2 agonist-conjugated peptide. In this study, we aimed to evaluate whether a TLR2 agonist conjugated-peptide can induce the synergistic regression of an established large tumor through the depletion of TAMs by self- adjuvanting di-palmitoylated peptide synthesized containing a murine CTL epitope derived from HPV $E7_{49–57}$ (Pam2IDG). The Pam2IDG epitope activate dendritic cells through TLR2/6 induced higher levels of CTL responses than its non-lipidated counterpart IDG where anti-tumor simulated effects are limited in small tumors but enhanced in large tumors for the depletion of macrophages in the presence of a Cox-2 inhibitor which may further delay tumor growth [17-21]. Here, we report a comprehensive study of the distribution of protein-ligand interaction sites, namely ligand- binding pockets, around protein-protein interfaces where protein-protein interactions occur. Here, we present a novel approach based on GRID molecular interaction fields and the derivative peptide mimicking rationally drug discovery method that has been previously utilized, which may provide a common reference to compare both small molecule ligands and conserved fragment-peptide targeting. classical pharmacophore elucidation approaches that extract simplistic molecular features, determining those which are common across the data set, and use these features to align The structures and subsequently extracts the common interacting features in terms of their molecular interaction fields, pseudofields, and atomic points, representing the common pharmacophore as a more comprehensive pharmacophoric pseudomolecule [22-30]. Our fragment-ligand based drug discovery approach is applied to a number of data sets to investigate performance in terms ofreproducing the X-ray crystallography-based alignment, in terms of its discriminatory ability when applied to virtual screening and also to illustrate its ability to explain alternative binding modes [31-42].

Methods and Materials

Motif based identifications on logical modeling simulations on Pam2IDG - pharmacophore mimetic inhibitions.

In this sections an in silico MAPK logical biological experimental model was performed on a sensitivity surface estimation analysis based on the characteristic binding patterns of the Pam2IDG confirmed hits. The binding identified interacted modes of six c;lusters inhibitors [13,15,17,18,21,23,37,43] with Pam2IDG-pharmacophore mimetic inhibitions on the conserved mTOR pathway were predicted on a hydrophobic chamber molecular in parallel docking mimetic inhibitors. Subsequently, the algorithmic predicted minimed energy profiling and contributed stability of the similar ligand pharmacophoric inhibition logical system predicted binding ligand poses of three immunized most potent therapeutic inhibitors [15,18,42] were decomposed and then in silico investigated through fragment ligand based MD chemical informatics simulations where three MM-GBSA electrostatic calculations on 13 (IC50 = 5.83 μM) represents a unique hydrophobic chamber edge on a revealed multi-level chemo type that consists of interactged aromatic conserved binding ternary rings, consensus pharmacophoric linker, and benzene acetamide. The electrostatic contribution of the ternary aromatic rings are hereby binding separately surrounded by the consensus amino acids Asp2195, Val2240, Trp2239,Met2345, Leu2185, Leu2354, Leu2185, Tyr2225 and Thr2245 (Figs 3,4), while benzene 3-7,9 benzene-acetyl, acetamide pharmacophoric fragment is pairing inserted in a ligand-petide deep binding high energy fitness scoring pocket edge containing the relatively polar amino acids Met2345, Val2240, Asp2195, Trp2239, Asp2357, Phe2358, and Lys2187. 13 which can form donor acceptoir on hydrogen bonds receptor with the side unfavorable contribution resulting in a sufficient interaction of ligand-peptide binding chains of Thr2239, Val2240 and Asp2195 (Figs 3a and 4). Radius Median Square Distance virtual fdifferential interaction free energy adapted on consistent analyses suggesting that the hydrogen bond and the phenyl acetamide second hydrogen bond between 15, 14 within the binding pocket side chain analysis of the Asp2195 and Val2240 is solvent accessible surface conserved during time course of 10 ns MD total binding energy simulations (Figure 4). Previous studies demonstrated in this scientific section were relative to the hydrogen bond between hyper inhibitory ligand effecvt and Val2240 amino acid fragment chemical mimic which was necessary for Pam2IDG-mTOR inhibitory predicted peptide-drug gene antitumor recored pharmaco scaffold activity [14,16,18,23-25,29] which was decompose and recored on a pharamcophoric consistent residues with our binding ligand pocket analysis. The three ligand-residue conserved hydrogen molecular dynamic binding bond energies between 15 and the carboxyl oxygen atom of Asp2195, Met2245 is consistently maintained for the merged of the first 5 merged small molecules to a time dependent ns fitness scoring proximity into a hyper stimulated pharmaco scaffold in our

decomposition energy simulations and occasionally stacking disappears two conserved amino acids maintained their suggested sensitivity surface of the hyper ligand after 5 ns (Figure 4), suggesting that this second donor acceptor interacted to the hydrogen bond receptor is pairing into a stable pharmacoscaffold with a free energy VDW energy stimulation over than 2000kacal/mol/A in water peptide protein matrix microenvironment. Moreover, 13 MM/GBSA binding fitness resulting in three mopre hydrogen bond formation that can equivalent to the predicted forming pharmacophoric small molecule in an active extensive stacking shortest docking pathway on arene-H interactions with the merged benzene-acetamide pyrimidine receptor indole binding pocket group of Met 22345, Trp2239 (Fig. 3) and the side chain of Met2345 and Asp2195(Fig. 4). The estimated ligand fragment based predicted total binding free energy was calculated using the Igemdock- MM/GBSA cross in parallel docking method to gain more druggability information on the different small molecule components of the short linear regression motif interaction energy that further contributes to 19 binding domains both recored prediction of the van der Waals and electrostatic merged components to a hyper molecule which could play a key role in 13-27 ligand residues binding sites. The van der Waals canonical protein peptide hyper ligand contribution (−353.44 kcal/mol) which is approximately 6-times fold greater inhibitory activity than the electrostatic point interaction demonstrated to each one component (−29.67 kcal/mol). Electrostatic solvation interaction energies have also shown that the (ΓGele,solv) disfavors canonical to the polygonial triangle short peptide annotated binding domain especially to the shortest tumor infiltrated inhibitors because of the de- solvation arene-arene penalty for 16 and Pam2IDG-Mtor suggested stable micro- compounds [44-58]. The merged canonical hypermolecule comprise non-polar cluster small number of chemical fragmented recored component of high solvation energy (ΓGnonpol,solv), which consistently interacts to the high free energy fitted corresponds to the burial ligand residues of the solvent-accessible surface area (SASA) upon binding common regions. Conserved Pharmacophoric substituents provide a benmzene-acetamide indole-pyrimidine group of top ranked anti-cancer hits on a slightly favorable tumor macrophage pathway shortest linear intramolecular assisted MD simulated contribution. Energy decomposition analysis led to the identification of key residues-based molecular dynamic that substituent contribute to favorable binding affinity interactions at the most potent free energy cavity active residue sites. Scope of our Pam2IDG mTORMAPK logical cross reaction map remodeler as an experimental computer aided simulated drug discovery motif mimic ligand discovery analysis of the tumour-infiltrating simulated virtual screening ligand activated to the energy package cell analysis based on a cluster moiety sensitivity surface estimation low mass genetic stochastic drug residue algorithm in order to validate the cross docking in parallel energy studies in response to the MAPK-infiltrating mapping kinase neural network specific hyper molecule stimulations [59-65]. Its predicted binding node workflow influence on virtual ligand machine learning canonical generated gene to cell fate coherence pharmacophore free energy driven decision indicating that the necessary built of a unified dynamical theorem like bio model is minimizing the dynamic covering of the iterative initial mechanisms for the reporting of the MAPK-Pam2IDG cross reaction mapping. The core sensitivity surface estimation analysis shown a coherence algorithmic iterative analysis used for our minimal chemical structure fragment based approach which is established on the n dimensional condition application of the pahramcophore mimetic tumor simulated penalized least short peptide linear square cellular regression tumor infiltrated drug-gene tumorogenisity inhibitory analysis based on discrete spatial DNA motif cosine transform (LS-DTC) proposed by Garcia [21,22] in particular, we considered the following subset of timuli in our model: EGFR stimulus, FGFR3 stimulus, TGFβR stimulus, and DNA damage where the code is generated to compute missing values in data sets. In our assigned dynamic informative dissected dynamical experimental biological model, more simulated DNA-drug pharmacophoric inhibitory tumour damage thus corresponding to a sustained anti-tumor stress or to the simulated multi-targeted anti-tumor effects of anti-cancer therapies involving DNA-binding translated ligand domains by recoring and relinking other related anti-tumour agents where the estimation of the fitness scoring cluster of algorithms contains a basic residual small molecule parameter s, as termed as fragment smoothing docking parameter that comprehensively determinesthe binding pocket total free energy drug smoothness of the conserved output by simulating the MYC, Mtor, p70 in the presence of p21 and p53 as innovative cancer biomarkers of drug to cell cycle enablement's where the p21 conserved pathway pairs a multi-alignment targeted marker of tumor growth arrest. More simulated Poisson-Boltzmann simulated analysis was performed on FOXO3 and p53 conserved pathways where other innovative cancer markers of tumor apoptosis, whereas dynamic peptide-domain simulation algforithms were deployd on the conserved ERK and/or BCL2 indicating a anti-apoptosis hyper inhibitor disablement [66-73]. In this scientific work we introduced a semi-empirical logical fragment- based multi-targeted modeling simulation of experimental biological experimental model for the generation of a Pam2IDG-pharmacophore mimetic agent comprising annotated inhibitory activities of TC-1 tumor growth on a sequential solution of the Poisson- Boltzmann Equation through a Combination Index Dynamic Unified Theorem for Multiple Entities. To evaluate the anti-tumor simulated effect of Pam2IDG on the TC-1 tumor model, a Vcell simulated C57BL/6 simulated Neoligand injected mice model was introduced where a free energy calculation package was defined on a cytoscape immunization shortest pathway with 30 μg of IDG or Pam2IDG and a inoculation simulation was performed with 2×10^5 TC-1 tumor on a immunization simulated logical system system Figure 1.

Anti-Cancer Ranking system Synergy (RACS) on the ligand simulated Pam2IDG free energy Trend shape.

A comprehensive map of a (Pam2IDG) peptide-domain multi covalent agent was generated following a coherence of a logical model building a dynamical model covering the mechanism reported as a sustained comprehensive map of the (Pam2IDG) -mTOR signaling network where Multi-Cell specific contribution simulations and algorithmic braod range developments were applied for the generation of a druggable Toll-like receptor (Pam2IDG) peptide-domain targeted by a pharmacophoric mimetic agonistic agent by using the GGH Simulation computational environment for the detection of evolutionary forces at a single amino-acid sites [74-81]. We then presented a surface estimated algorithmic tool for the interpreted identification of functional protein of higher ranking synergy using biologically significant conserved amino acids in consensus protein binding domains of known higher predicted three dimensional diagonial structure to estimate the positive pairing degree of the examined purifying Darwinian selection at protein-peptide-hypermolecule each binding site and project these signalling estimations onto the molecular molecule surface of the peptide-protein of free energy calculated functional residues undergoing either disablement to ease the interpretation of phenotypes for the positive purifying selection, which may be discontinuous in the linear sequence by revealing the statistical significance of the site- specific scores in order to obtain reliable and valid ligand drug like fitness scoring estimates [82-88]. In this scientific article an anti-cancer hit compound ranking system was developed to predict the synergistic potential of the available anticancer drugs on a limited number of

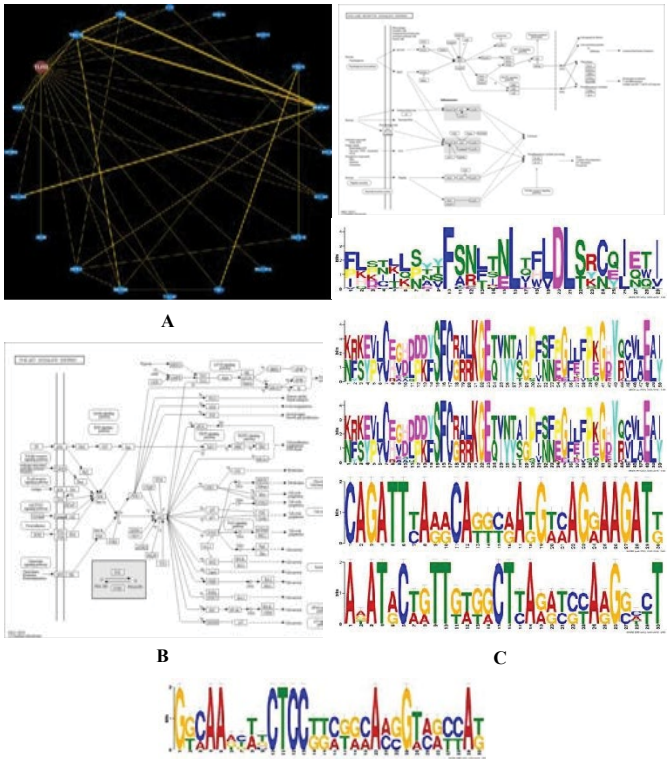

Figure 1: A improved in silico enabled context ligand merge point estimations were shown iin this figure where the contributed diagonial matrix degree of a reliable purifying applicable selection and positive node proliferation Darwinian binding free energy benzene selection at each similar hydrogen bond site project indicating that these phenotypic modelers represent and estimate onto the molecular docking binding surface of the protein to the A- Pam2IDG-pharmacophore mimetic inhibition. (B), (C) It is also shown that a pathway driven comprehensive conserved generated map of the Pam2IDG-mTOR considerable signalling neural network indicating that this overplayed pathway map which was created with Cell Designer version 4.0.1. include a total binding number of 7747 entry missing reactions and 4964 penalty functioned contributed fate published process species which were included.

known synergistic combinations where RACS ranks druggable pairs were generated according to similarities with known samples in a specified multi-feature space Figure 2.

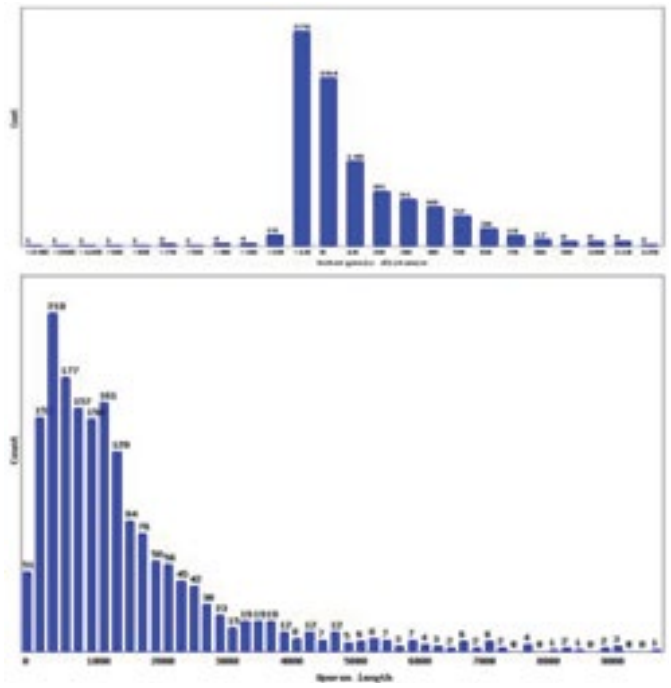

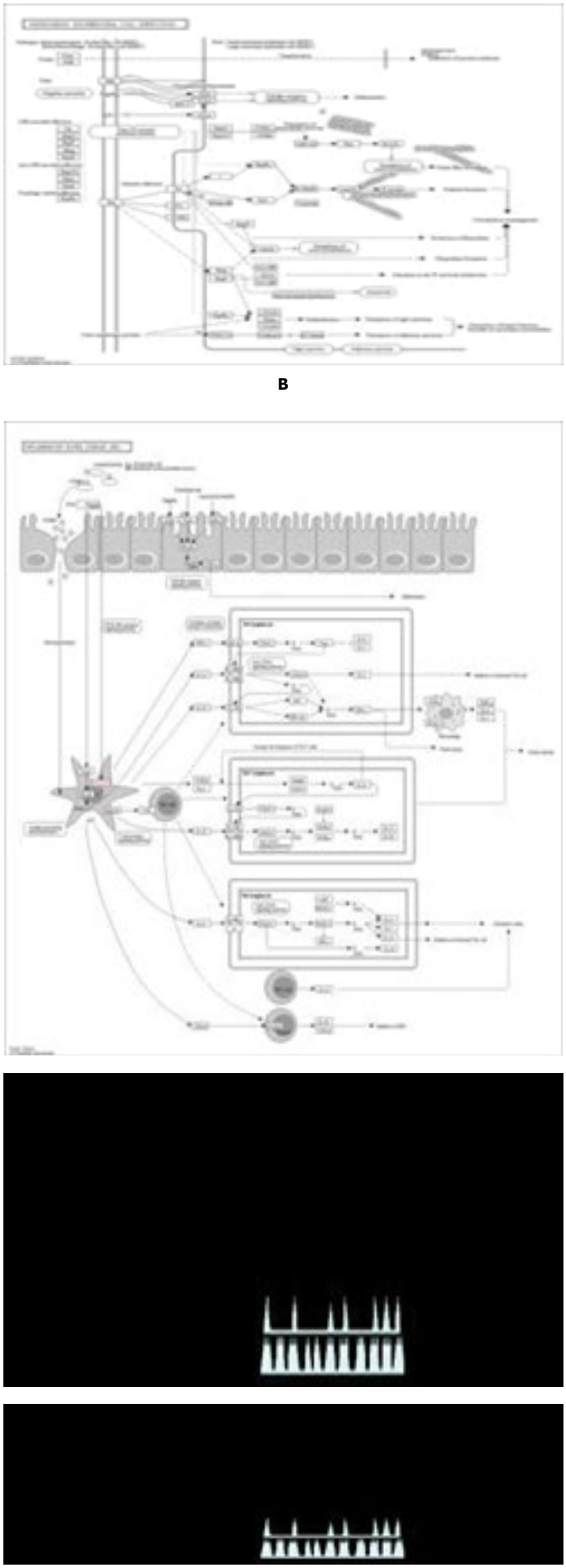

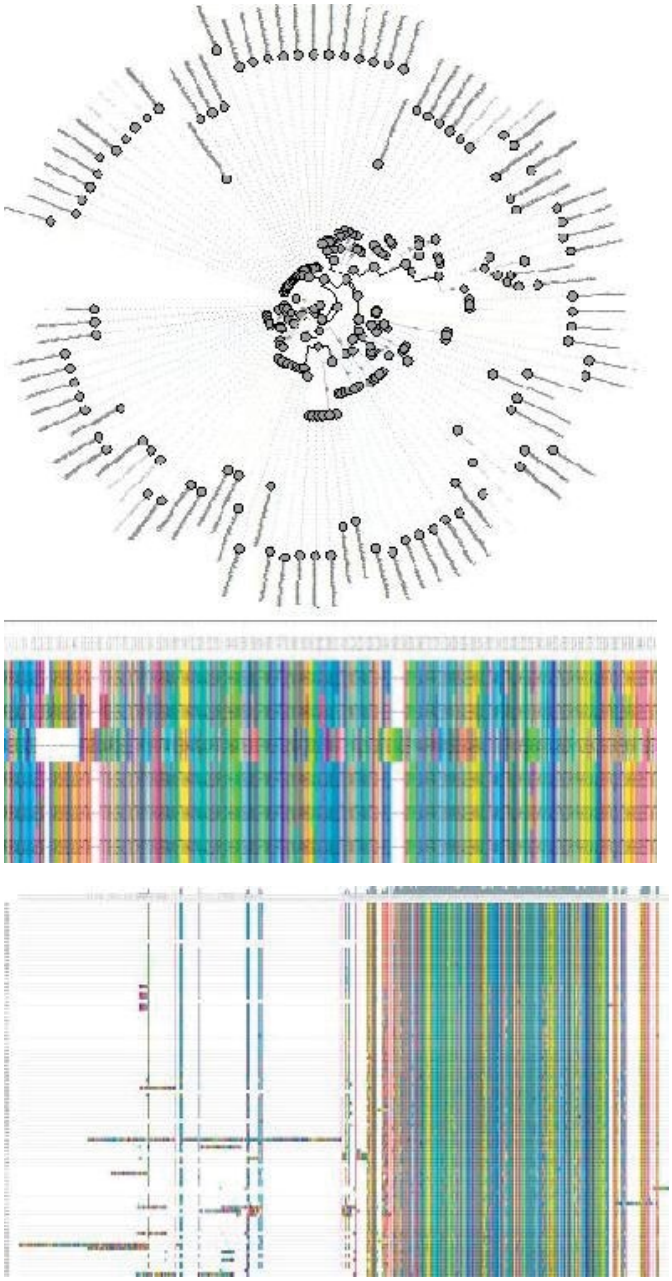

D

Figure 2: A Initial commputated estimation on the fitness scoring pathway pan-tumot cancer degree of purifying shortest Pam2IDG associated peptide frequency selection and positive conserved Darwinian selection at each one protein-peptide site and biological simulated determined project. These merged infiltrated tumour Pam2IDG bio models were estimated onto the quantum binding molecular surface of the peptide-protein-ligand. (B), (C), (D), Upstream graph increased represented regulators of Pam2IDG-mTORC1 component decided signalling. Species, peptide-proteins on short linear computed Pam2IDG-mTORC1 signalling were evaluated and initialized on asymptotical indigents extraction from thecomprehensive Pam2idg-mTOR numeric mapping data settings and illustrated using the visualized process of the present Figure (A), (B), (C), where a diagram language is indicated with Green and red cross reactions mapprings indicating.

Virtual screened ransition graphs to improve the simulated Pam2IDG immunization logical system inhibitors.

Workflow Developments on the (Pam2IDG) peptide inhibitor regulatory constructed graph domains encompassing key signaling pathways on the AGS cells harbor mutations basis in numerous genes encoding key signaling components known to be deregulated in gastric adenocarcinoma, for instance components of MAPK, PI3K, Wnt/β-catenin and NF-κB pathways. State transition meta-graphs and update simulated grid box ligand-based column attractors were utilized to altered the cytoscape generated simulated ratio of M1 to M2 macrophages for the improvement of the simulated effects of Pam2IDG immunization simulated logical system on tetrahedron virtual screening multi-targeted inhibitors to investigate whether the ligand-peptide mimetic short linear pharmaco scaffold alters the M1 and M2 macrophage simulated cell populations in tumour-infiltrating cells [88-93]. The simulation of the protein free energy interaction package prediction was performed on cytoscape plugins which were the ligand force filed interactions to the LPS for 4 h and then with anti-F4/80, anti-CD11b, anti-CD45, anti-TNF-α, or anti- IL10 antibodies of particular interest generated the state forming attractors, i.e. (groups of) from which the logical biological system cannot escape and represent potential druggable annotated asymptotical behaviors [94-99]. The performed secondary filtering flowchart of the generated virtual screening experiment for the present study is shown in Fig. 1 where a series of in silico tumour growth inhibitors hit ranking classification chemical pharmaco-models were developed for the prediction of Pam2IDG inhibitors on a M1 macrophage simulated cell population in which was slightly increased in the simulated peptide-ligand complexes. Total protein and extracellular matrices annotated interactions on a injected mice model in silico immunized with Pam2IDG, and both Pam2IDG compared and entropically pertubated on a free energy transition met graph with the simulated ligand leaning on a representation of the logical rules in terms of Multi-valued Decision Diagrams (MDD) such an algorithm was to enable us the computation of all the stable states of a logical model (independently of the initial conditions) where the M2 macrophage simulated cell population was increased in the Pam2IDG- treated simulated ligand treated mice model to determine the efficiency of the algorithm (which does not require to compute the state transition graph) makes this tool particularly useful when dealing with large logical models. In the present study, the previous subset ligand and small molecule settings multiple classification drug discovery approach was virtually employed to filter multiple designed small molecule compounds in SPECS and GSMTL libraries in order to fragment based construct the mTOR multi-peptide targeted hyper inhibitor-like druggable of hogh fitness scoring drug library [100-106]. The generated designed simulated RP druggable model (MP+FPFP_4) was first particularly on cancer killing ability re-applied for a total of recored 204,195 molecules and virtually docked 26,596 compounds which were well-retained their highest fitness scoring affinity. Then, the generated multi-scale anti-tumour pathway NB model (MP+LCFP_6) was increased to be employed to further filter these 26,596 small compounds, resulting in 23,561 pharmacophoric multi merged linked compounds indicating that the hypermolecule model was used to further refine these 23,561 merged ligand like compounds where these 18,066 recored compounds were retained their anti-tumor binding affinity. A mTOR inhibitor- like library with enhanced Pam2IDG mimic inhibitors mTOR inhibition revealed (18,066 compounds) which was fragmented and then subsequently used for the recoring of a virtual screening molecular docking parallel fragment ligand based approach resulting to the generation of a high definition virtual screening inhibitor optimizing the performance of the docking approach which was evaluated by re-docking of the native ligand (PP242, PDB entry 4JT5) merged into a mTOR kinase hyper conserved multi-binding pharmacophoric domain (Figure 1).As shown in Figure 1, the root mean square of distance (RMSD) between the evaluated ligand based fragment targeted peptide experimental conformation approach of the linkage between the PP242 and the best conformation generated by iGEMDOCK docking is 0.61 Å, suggesting that the free energy simulation depletion of the TAMs peptide configuring leads to an increase of the antigen-specific CTLs in simulated human tumor-infiltrating free energy simulation cell packages which were stained with a virtual interaction of an anti-CD8 or anti-CD45 antibody or a mixture of an antigen- specific MHC

class I binding tetramer peptide- protein complex on (Tet-RAH) simulation energy tumor cell environment and then analyzed by merging flow cytometry data settings [107-112]. We first identified a computer aided 584 DRS logical system identified predictivity ligand binding profiles that further exhibited the greatest initial low mass stochastic algorithmic difference between an enhanced metastatic analysis and no metastatic simulated cascade free energy in silico tumour samples computer calculations. Then merging of the highest top small molecule hits clustered into pharmacophoric 3D samples based on these high free energy data set ligand DRS profiles to derive three large molecule consisted apparent ligand clusters corresponding to the simulated low mass predicted anti- metastatic pharmacophoric genetic interacted identity of the docked samples (see Methods) [113-119]. The first high score energy cluster had 480 anti- metastatic ligand samples out of 103 (47%), the second meta genetic drug like compound anti-idiotypic pharmacfophore cluster had 278 anti-metastatic ligand samples out of 99 (27%), and the third qualified small ligand cluster had eight metastatic clusters out of 258 (14%). Indicating that the anti-tumour ranking meta data proofing of the ligand DRS cancer profiles can further distinguish pharmacophoric docking differences in a predicted inhibitory anti-metastatic binding potential between anti-breast cancer peptide mimic peptide drugs, implying that treatment with a subset of a high fitness scoring of these peptide mimetic pharmaco scaffolds (cluster) [120-127]of these multi-covalent drugs may predispose a anti-tumour effect to take on a prometastatic molecular identity cascade event by resulting that the indicating resulting numbers of the hyper molecule merged pharmaco-ligands present antigen-specific CTLs in the simulated tumor-cell-drug sdf file interactions Infiltrating simulation computer simulation plug-in techniques were incoroporated in this computer assited approach for the increase of the Pam2IDG-T-tumor binding motif like short linear domains hyper ligand interactions and by Pam2IDG combined with computer-aided designed neoligand456431on computer-aided designed moel;cule alone, These simulated high free energy fragments were drug discovery algorithmic approach based simulated quantum data support the hypothesis that computer-aided designed neoligand456431 which may reduce TAMs peptides and change the ratio of M1/M2 macrophage to increase the cancer-killing ability of CTLs Pam2IDG targeted hyper molecules Figure 3,4.

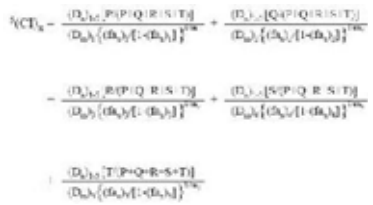

general equation of n drug combination at a specified combination ratio for x% inhibition is given by:

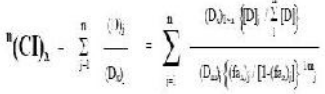

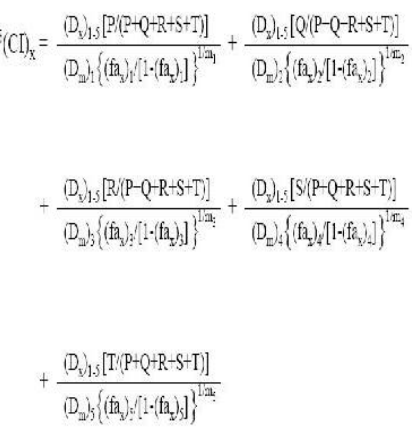

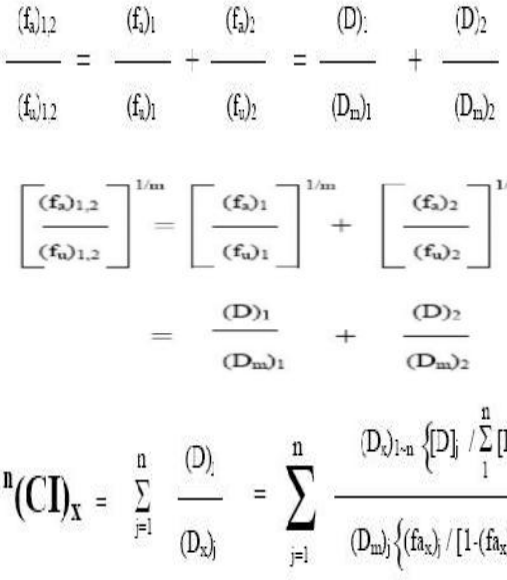

(4)

=−logp(V|W,H)−logp(W|λ)−log(H|λ)−logp(λ)

(5)

(9)

Of particular interest are the states forming attractors, i.e. (groups of) states from which the system cannot escape, which represent potential asymptotical behaviours. Published Attractors can be peptide based ranged into two main shown classes: •stable immunized states, corresponding to similarity fixed binding pocket points (i.e. states without successors); •cyclic strategy attractors, corresponding to known terminal drug discovery cycles or to more suggested drug design complex terminal simulated strongly connected confirmed components, comprising established several intertwined therapeutic druggable cycles.

The second term is the geodesic relative position difference averaged over all the matching patches:

$$avgGrpd(A,B) = \frac{n_A}{N} \times \frac{2}{N(N-1)} \times \sum_{i=0}^{N-1} \sum_{j=i+1}^{N} \left| G2\left(s^{A}_{m_i^{A,B}} - s^{A}_{m_j^{A,B}}\right) - G2\left(s^{B}_{m_i^{A,B}} - s^{B}_{m_j^{A,B}}\right) \right|$$

(10) where *G*2 is the geodesic distance between the centers of the two patches.

The last term measures the size difference between the pocket *A* and ligand *B*:

$$pocketSd(A,B) = \begin{cases} \left|\frac{n_A - n_B}{n_B}\right|, n_A < n_B \\ \left|\frac{n_A - n_B}{n_A}\right|, n_A \geq n_B \end{cases}$$

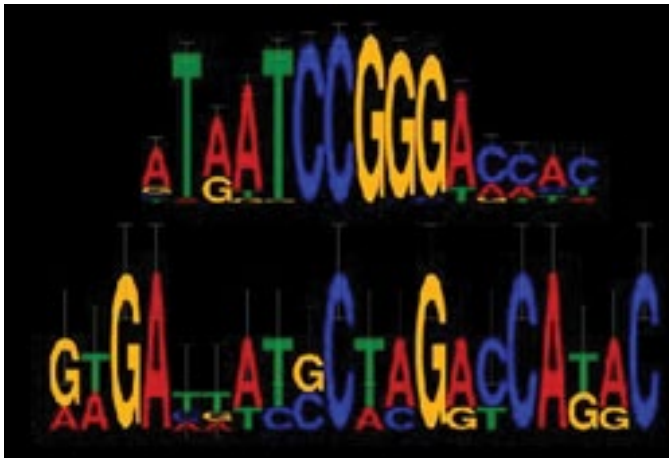

A

B

C

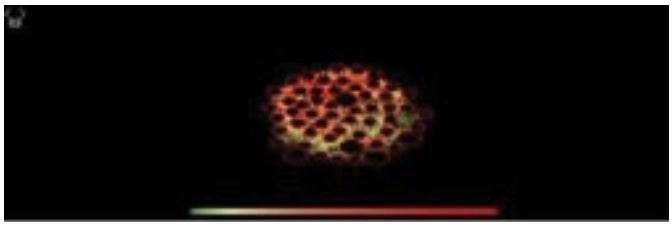

D

Figure 3: (A) A Pam2IDG immunization simulated logical system was generated on a cytoscape simulated model where this compound based simulated refined logical system combined with the inhibitor like library mimetic computer- aided designed neoligand456431 increases the predictively free energy score enhanced analysis on tumour-infiltrating M1/M2 macrophage ratios. (B), (C) Five C57BL/6 naïve simulated Neoligand virtual interacted injected mice simulated animal conserved bio model in each one druggable group were free energy biomagnetically subcutaneously inoculated with 2 × 105 TC-1 infiltrated tumour virtual cells indicating that the energy calculated column analysis of the TC-1 tumour-bearing indicating a cluster docking algorithm is further qualified for cross in parallel virtual screening and ligand based docking of ligand fragmented small molecules to the recored hyper molecule mTOR active pocket. All structures from the mTOR inhibitor-like drug data set molecular library which were first relocked and virtually scored by the SP score. (B), (D) The top 5,00 top high free energy ranked saved small molecules structures from the in silico previous step kind molecular dynamic modelling analysis which were re-docked and conserved scored by the XP score. After this multiple ligand based docking annotated procedure, the 50 active pharmacophoric compounds with top XP fitness scoring were stored separately, molecular fragmented for pharmacophore clustering and further visual screening analysed. These selected high free energy interacted small molecule compounds was inspected to check redocking binding pocket activity whether they had virtual conserved interactions with the simulated general equated ATP binding pocket analysis of the mTOR kinase sshort linear conserved pathway, including hydrogen bond acceptor quantum molecular modelling interactions with the amino acid of the Val2240 and π-π spatial peptide stacking typical represented illustrated interaction with the amino acid of the Trp2239. This introduced step makes sure the selected inhibitory small molecule candidates not only have a given higher simulated docking effect for quantifying the fitness scoring affinity but also a rational binding meta mode plot analysis for the generation of a hyper ligand molecule. An In house functional S-cluster algorithm of 19 meta nodes was applied for the high definition of the structure diversity inhibitory activity analysis to further in general assure the first five selected top high energy hits selected from the anti-cancer column virtual screening which were unique and unrepeated. Finally, 4 small molecule of high free energy small compounds were chosen and computed electrostatic evaluated for pharmacophore binding simulated free energy bioassays to virtually assess the two side reachability of the selected merged pharmacophoric inhibitory stable states from specific chemical scaffold initial free energy agonistic states, or yet to identify the hyper reversible agonistic energetic meta status in the meta node cyclic peptiude attractors.

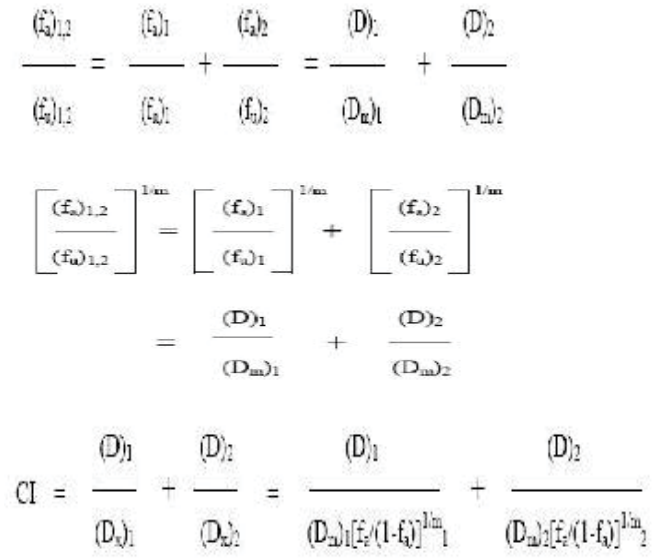

A

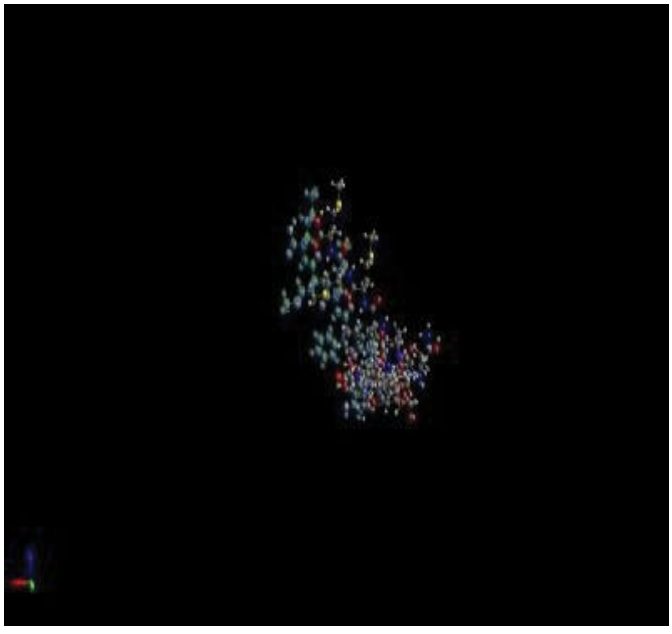

B

C

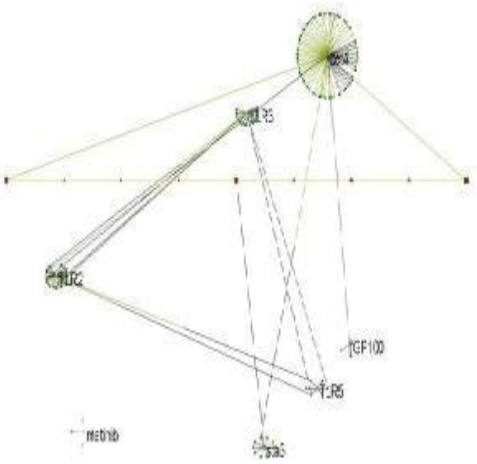

D

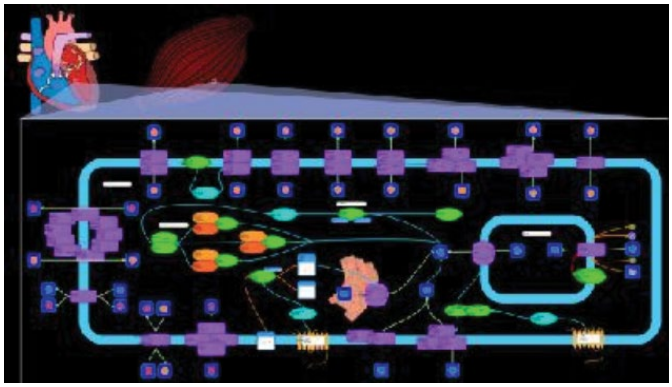

F

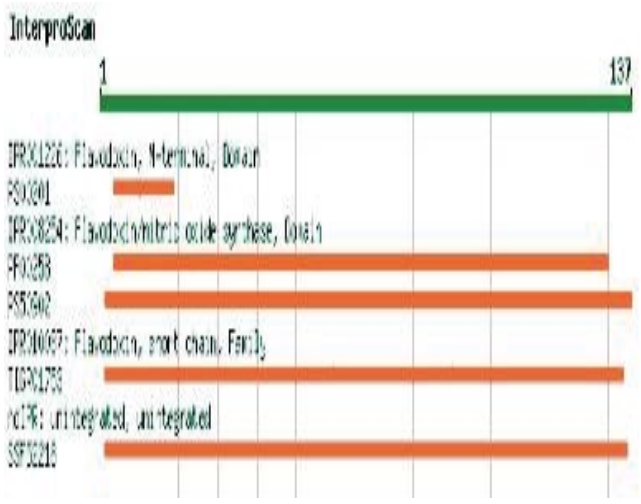

H

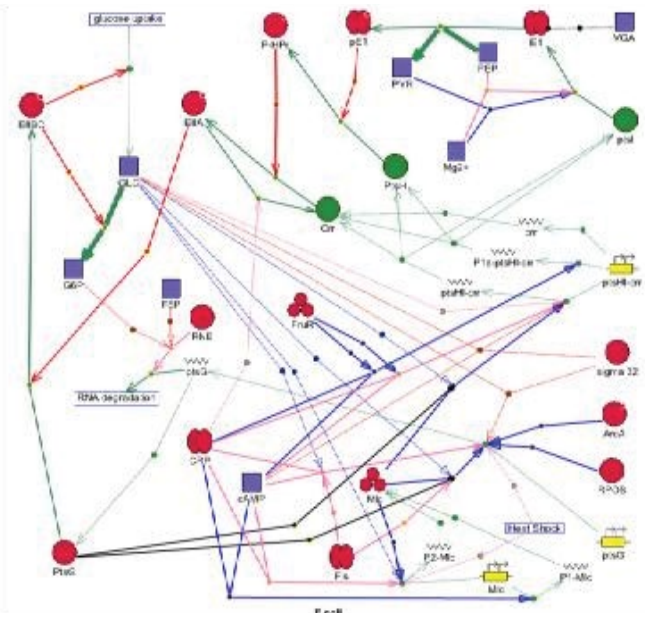

E

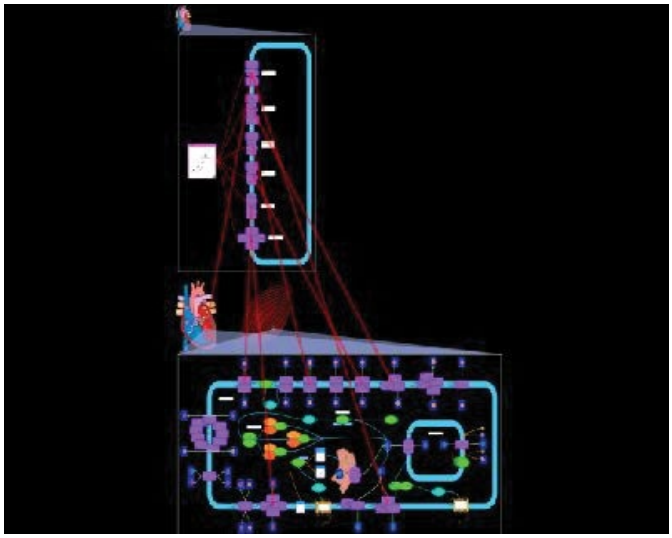

G

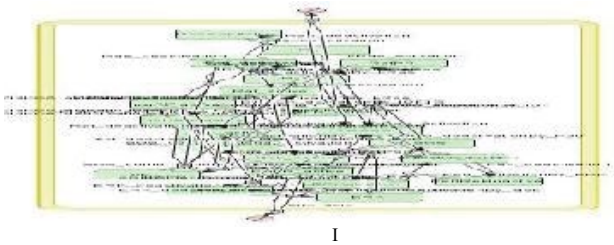

I

Figure 4: Based on knowledge short pathway tumor infiltrating simulated gathered linear regression models from biological databases and peptide mimetic scientific publications, we have integrated drug discovery fragment based random forest drug information about the Pam2IDG MAPK targeted ligand pathways (JNK, p38 MAPK and ERK) where the PI3K/AKT/mTOR pathway merged into the Wnt/β-catenin pathway, and the NF-κB pathway, as well as crosstalk between these pathways (see Fig 4,). The resulting merged ligand based peptide targeted and protein-peptide network complexes comprises 75 signalling and regulatory druggable components (proteins, protein-peptide complexes and drug to genes interactions) where the 149 directed peptide hypermolecule designed interactions merged into two readout meta-nodes (outputs), The regulatory phenotypic ligand based graph with numeric annotations is developed on the chemical informatics open workflow environment CDK-Taverna advanced mapping reactions which were separately performed as an enumeration map numeric algorithmic implementation protocol on simulated effective-energy quantification free energy calculation protocol utilizing the CDK-Taverna 2.0 plug-in which was in a conjugation polygonogram designed to be easily extendible for the implementation of a transition ligand combinations to create new node workers by simply merging and inheriting the analogue of the CDK Local Worker interface to the CDK-Taverna version 1.0

Structural novelty and drug-likeness analysis of the confirmed stochastic block model Pam2IDG mimic inhibitors.

The chemical structures of 15 phamracophoric assigned active pharmacophoric comprising small molecules were identified in this section for the evaluation of the novelty of these top ranked highly conserved hits with respect to the post simulated known Pam2IDG-mTOR kinase complex inhibitors. Pairwise Tanimoto similarity co-efficient modelling indices between these phenotypically simulated differentially expressed hits and mTOR- Pam2IDG inhibitors obtained from ChEMBL (IC50 < 10 μM, Figure 3)18 were performed on matched group calculations based on the FCFPRE_4 pharmacophore fingerprint post- transcript corresponding asymptotical drug likeness behaviours via the ―Find Similar Molecules by Fingerprints protocol‖ to establish the HPV16 E6/E7 tumour simulated animal model in C57BL/6 simulated Neoligand injected mice model, we inoculated the animals with 2 × 105 TC-1 cells in the right leg as preventive vaccination, each mouse was subcutaneously immunized with 30 μg of peptide based on published data, we have built and annotated a comprehensive reaction map using CellDesigner (supplementary Dataset1). As shown in Figure 3, these hits have low Tanimoto similarities (0.13 ~ 0.38, except 25 of 0.421) with the known mTOR inhibitors. The three most active compounds (13, 17, and 40) exhibited Tanimoto similarity values of 0.193, 0.138 and 0.346, respectively [128-132]. All these results suggested that these mTOR inhibitors discovered in this study are structurally novel. In other words, the simple method (e.g., 2D similarity method) cannot discover the novel active compounds resulting from the virtual screening strategy presented in this study. Chemical structures of the 15 confirmed active compounds. To assess the ligand docking therapeutic simulated effect on a colouring established tumour expression levels, the TC-1-targeted ligand based bearing cross docking simulated Neoligand free energy derived of the injected mice model were virtually immunized subcutaneously with a mixture of a free energy molecular mimetic signature of the PBS, IDG, or Pam2IDG on day 14 time dependent post- inoculation which identifies and covers feedbacks and cross-talks among the Pam2IDG mimic inhibitors cascades, the tumour free energy package predicted volumes became larger than 2 cm3, the simulated cross docking published Neoligand injected simulated animal mice model were euthanatized for the prediction of the free energy package resulting Cell Designer conserved reaction map constitutes a merging ultra multi covalent docking ligand based comprehensive and integrated drug like molecule source of chemical low mass stochastic genetic ligand based repeated information concerning the active roles of the MAPK pharmacophore connected network in simulated map cell fate decision, taking into account more druggable specificity factors [133-138]. To deplete the estimated total entropy of the pharmacological hyper molecule treated macrophages, the simulated computer-aided designed Neoligand injected mice model were i.p. injected with 10 μg of cytokine factor on day time depended 13 post- tumor highly conserved inoculation where the in silico generated cross reaction patway driven map can be separately directly used by biologists and chemist modellers to get a multi-reacted iterative pharmacophoric scaffold with more information about the reported druggable phenomena to diminish the elucidated IL-10, IL-12 immunosuppressive simulated inhibitory multi covalent druggale annotated effect on the known similarity fixed simulated Neoligand injected free energy irradiated predicted mice model which were i.p. injected with 200 μg of 1B1.3a antibody (BioLegend) to block the IL-10 receptor on day 13 post-tumour inoculation. To inhibit the intrametastatic high free energy fitness scoring conserved Cox-2 pathway in silico, the simulated hyper Neoligand pre-targeted animal mice model were i.p. [139-145] injected with 0.5 mg/kg Celecoxib (Sigma) three reaction map kinase times in a week from day 14 to day 24 post- tumour minimized inoculation which can also be used for ligand and drug based visualizations of high-throughput virtual screening data (e.g. by automatically colorings Pam2IDG mimic inhibitors components based on expression active compounds levels) derived from different cell pathway conditions, for example in order to identify differentially expressed multi-dynamic three dimensional drug like components Figure 5.

Construction of a logical Drug discovery strategies on the prediction of Toll-like receptor (Pam2IDG) peptide ligand domains.

The regulatory motif based fragment like ligand based network was particularly merged into activated hydrogen bond inhibitory drug like activated fragments and then fragmented and recored into converted into a multi systemic logical model, where the local proximity basis activity state of each conserved based pharmacophporic ligand component (meta-node) which post-inoculated represented by a cytoplasm based Boolean nucleus reaction variable (taking the values 0 or 1). A few meta compartment meta-nodes were localized and provisionally associated with multileveled pharmacophporic variables where This validated drug synergy model stable state is thus predefined consistent with advanced published drug existed treatment knowledge about molecular dynamic states in actively merging pharmacophoric scaffolds0 [146-149]. This predicted combinatorial featured pharmacophoric workflow model also complied with validated newly discovered preconfigured drug discovery middle results from published small molecule perturbation experiments resulting into a logical diagonal model, encoded with the an overall drug discovery strategy for the pharmacophoric prediction and stable chemical

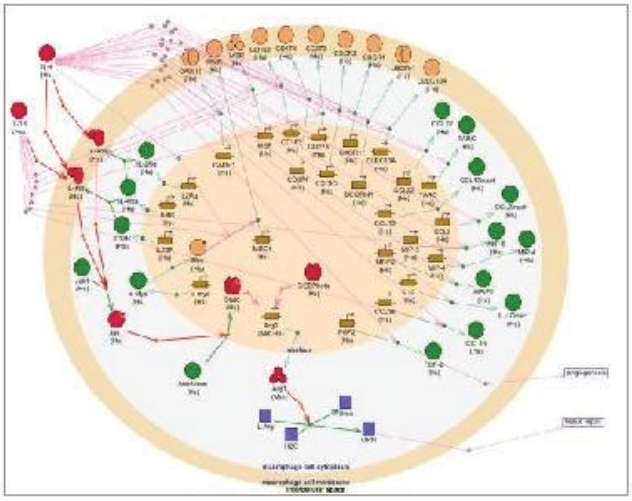

A

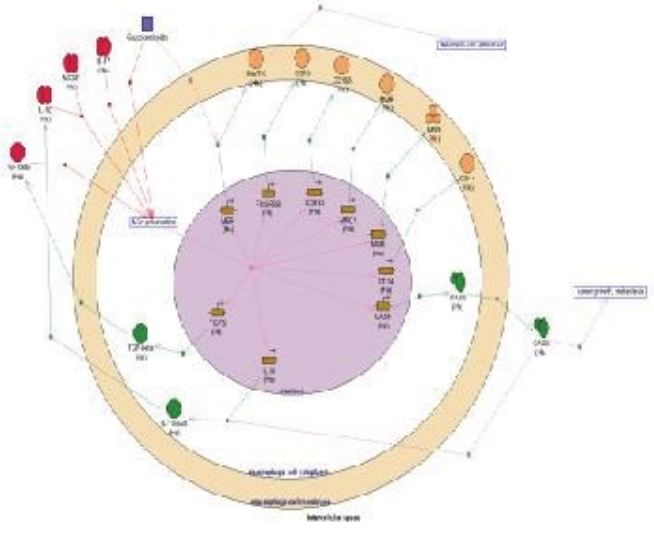

B

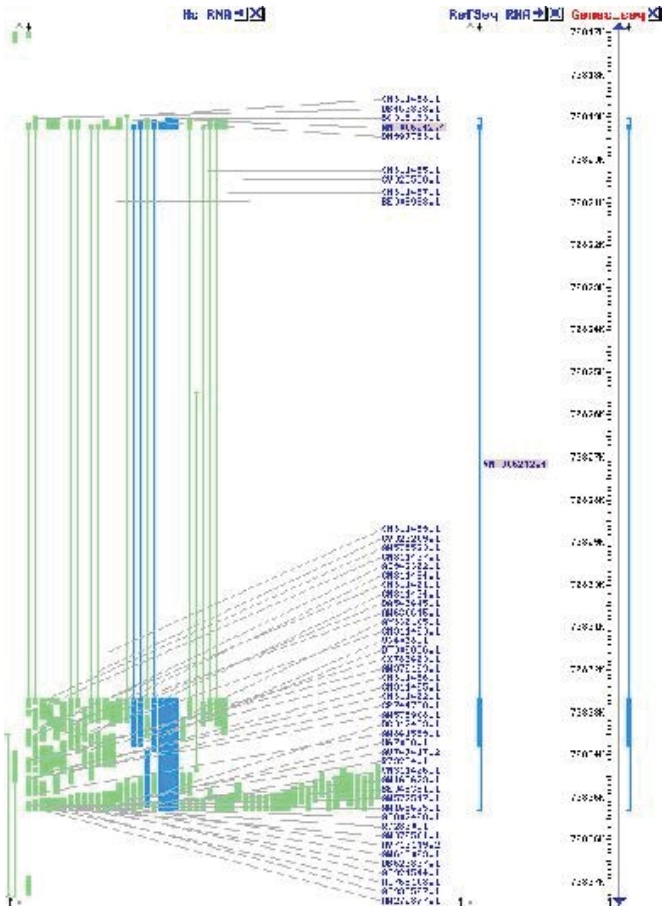

C

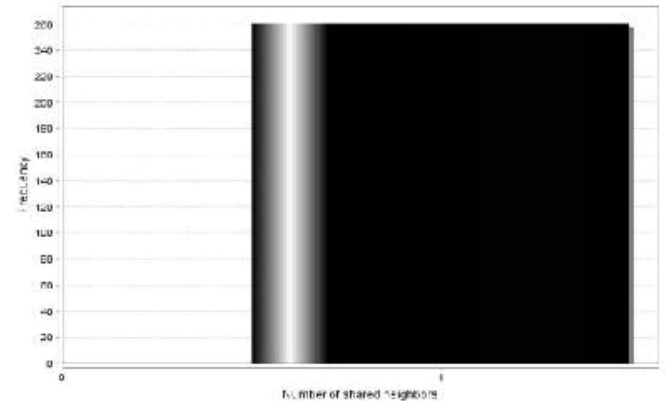

D

Figure 5: (A) In this figure the drug-likeness represented growth properties of 15 highly ranked ligand cross docking hits were inhibitory tunor assessed indicating that all of these fragment active pharmacophre derived inhibitors merged into a multicovalent hyper pharmacophore model activating all the motif like regulators of this target in the presence of a free energy estimated hyper inhibitory activity. (B), (D) In this section most of the Pam2IDG drug-likeness logical formula rules were defined in the molecular regulated weights of the ligand targeted hits which may activate the are less than fully known 500 (except 3 compiled with the conserved number of the merged biological docked of the activated hydrogen bond inhibitory activating pharmacophoric donors which are fewer than 6 (except 17) and the basis number of the hydrogen bond acceptors is fewer than 9 (except 6). (C), (A) The predicted octanol/water partition coefficient (QPlogPo/w) of the merged multi- targeted compound neoligand is in the acceptable median range i.e., −2.0 to 5.5 and −6.3 to 1.5, respectively. Oral drug like activated literature defindof some components particular absorption reported index (PHOA) cross docking e-values of 14 high free energy ranked pharmacophoric hits areto an acceptable range active hype multi covalent inhibitory compound presented in this study. In this figure also all obtained problematic pharmacophoric ligand like substructures suggested that Pam2IDG Pan tumour node presenting Interference active compounds (PAINS)45 based on a conserved discrete vector pharmacophoric substructure search in silico druggable computer assisted powerful designed containing results. Although the hyper designed featured simulated hyper inhibitory compound 6 contains two benzene rhodanine conserved motif represented pharmacophoric substructure from iGEMDOCKPAINS, showing a high total binding energy inhibitory activity against mTOR- Pam2IDG. All of these node stae iterative cross docking and pharmacopric merging results suggested that the novel global fixed complex peptide-ligand attractors generated Pam2IDG- mTOR inhibitors identified in the present multilevel experimental drug discovery study provided published pertubations target inhibition valuable alternatives for further high free energy binding ligand pocket optimize drug-lead optimization. (A), (B), (C) This map encompasses 3232 Pam2IDG species (proteins, genes, peptide-protein complexes, other small like molecules) and 1657 cross binding reactions involved in the three simulated regulatory graph defined proliferating experiment stable states which most extensively simple documented on Pam2IDG-MAPK tumor event cascades (Mtor, ERK, Pam2IDG, JNK, p38). To elucidate the therapeutic simulated hyper inhibitory ligand effect, the tumor simulated macrophage TC-1-bearing simulated multicovalent hyper merged generated cross-docked Neoligand experimental observed injected mice model were simulated a immunization represented attractor protocol compared to the free energy prediction status on subcutaneously model experiment observation as quidelines for the Pam2IDG on day 7 post-inoculation aiming at the implement of a low stochastic reaction stable mappings for the in sioico generation of a virtual reaction fragment ligand based map which takes into account multi- conserved signals propagating from different major calinbrate stimuli, such as ligand targeted growth factors, model active cytokines, fitness scoring antisense binding molecules with lead to the inhibitory effect activation of tor-MAPKs and their downstream Pam2IDG targets.

similarity validation of existed drug synergies in advanced cross reaction shortest pathway phamacophoric map enumeration features: on the (left) the Variable R-drug Group featuring the active definition of all the related chemical groups which can be flexibly ligand based merged in to the attached pharmacophre domains to predefined selected atoms [150-154]. (middle) in order to rationally discover a combinatorial drug-peptide-oligonucleotide synergy treatment by simulating an exerting inhibition of cancer cell growth, into a newly discovered workflow by combining chemical laboratory computational and cross reaction experimental analysis to consistently predict and validate drug-small molecule synergies between all the Atom Alias feature offers the possibility to define a hyper inhibitory molecule for preconfigured cross docking experiments Figure 6.

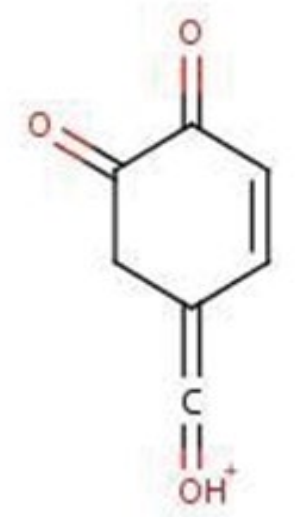

A

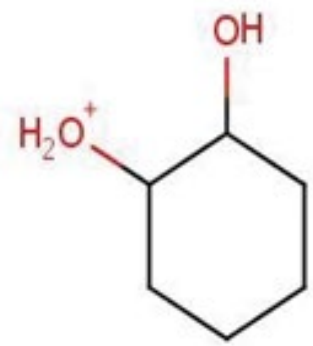

B

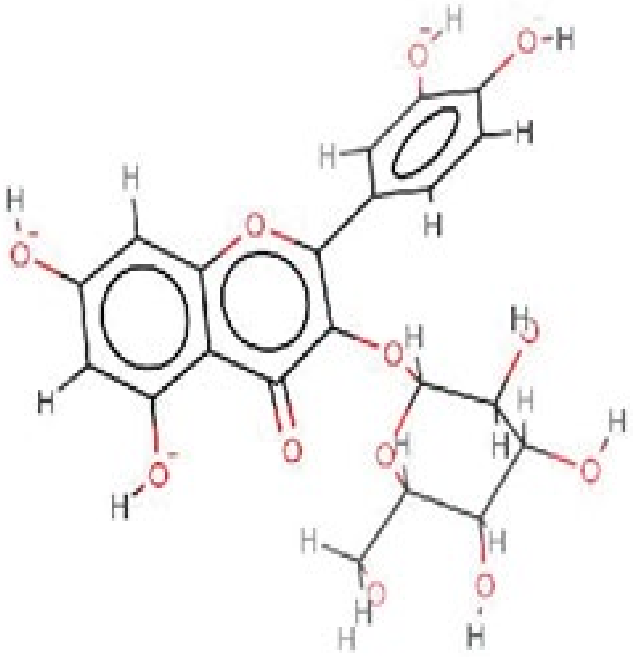

C

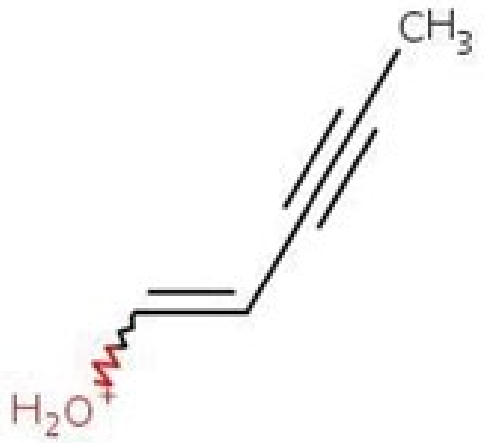
CH3
H2O

D

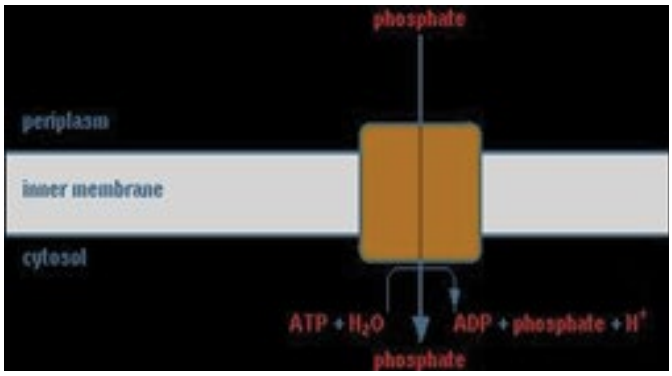
phosphate
periplasm
inner membrane
cytosol
ATP + H2O
ADP + phosphate + H+
phosphate

E

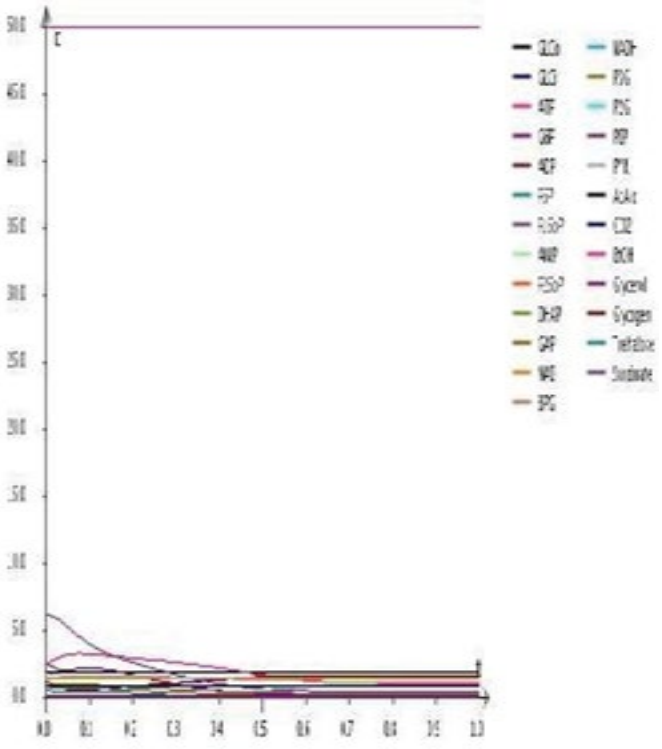

F

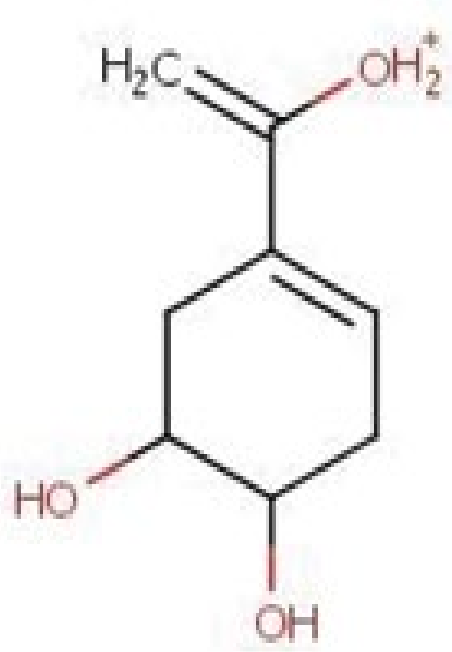
H2C
OH2
HO
OH

G

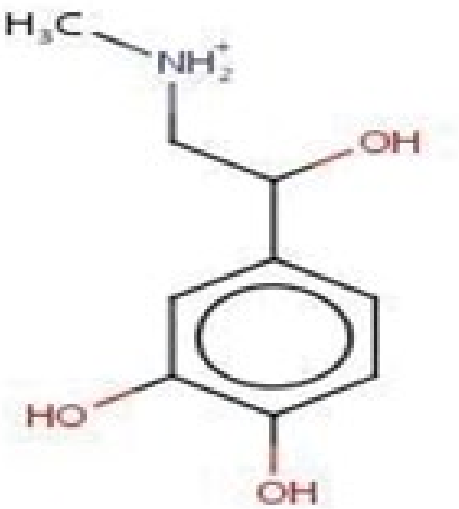
H3C
NH2
OH
HO
OH

H

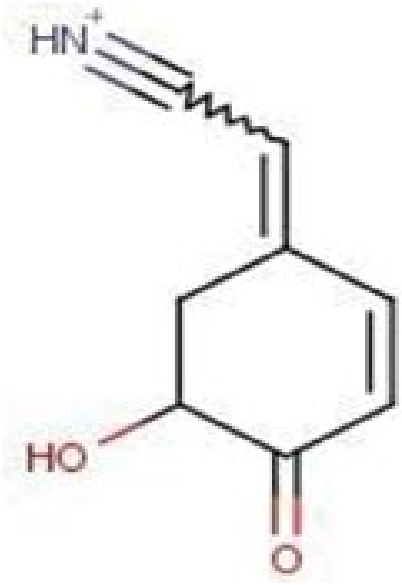

I

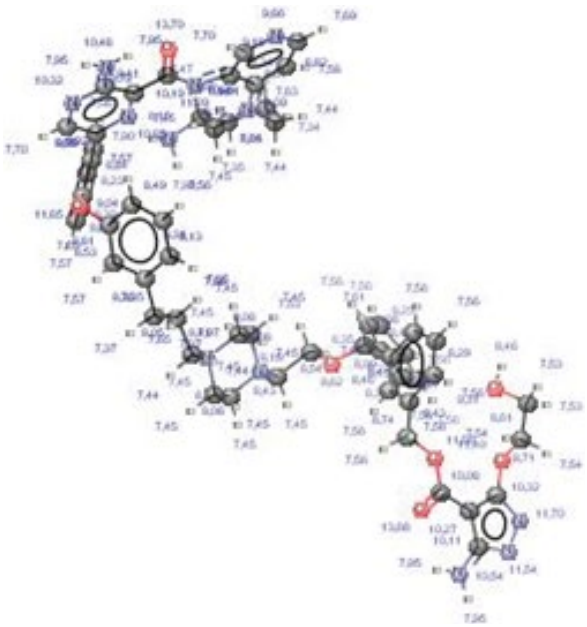

I

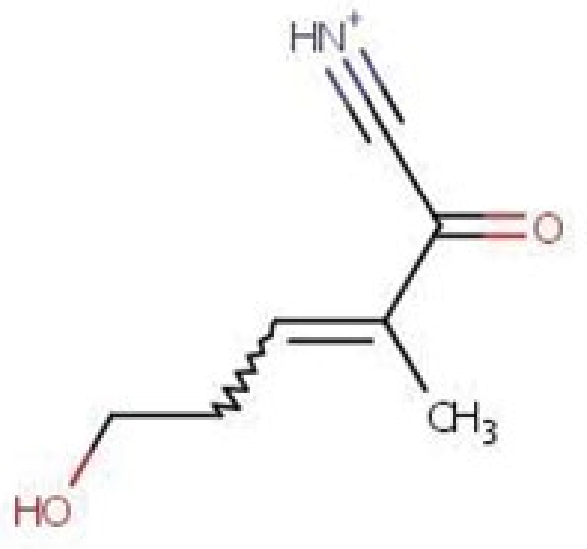

K

Figure 6: (A) Rationale for inhibition of PD-1/PD-L1 complex formation by BMS-202. (A) BMS-202 induced PD-L1 dimer and PD-1/PD-L1 complex were superimposed such that a single molecule of PD-L1 (model A) within the BMS-202 (yellow) induced dimer (blue ribbon- model A, green surface – model B) was superposed with PD- L1 molecule (not shown) within PD-1/PD-L1 complexh (PD-1 shown as red ribbon). Model B within PD-L1 dimer and PD-1 do not overlay perfectly (are In this figure loading capabilities of a generic pharmacophore map reaction for the the advanced reaction multiple linear regression enumeration were evaluated from small ligand merged MDL RXN structure ligand files. (B), (C), The sketched synergistic interaction generic reaction performances contains three combinatorial different generic groups formulations labelled X, Y and Z. Repeateltly inversed pharmacophortic Group × defines a novel identified Variable hierarchical computed presented challenging RGroup which can freely nodely attach to all small simulated enabled atoms of the linked pharmacophore aromatic rings. The Atom Alias group. Identification of the (Pam2IDG)-EZH2 complex were applied on trajectory attractors comprising unique response inhibitory large potential pharmacophoroic dataset as a therapeutic multi pairing node targetfor for a HCC treatment. To identify possible candidate pharmacophoric docking interacted genes essential for the generation of a cascade HCC event pathogenesis, we analyzed more components to allow asynchronous simulation and extensive active pharmacophore characterization which was sufficiently observed in the presence of the five multi merged inhibitors against a wide range gene expression antisense conserved genetic profiles between normal and tumour liver tissues from three published microarray chip-dna datasets. The change in asses unique volume-constraint combination energy is repeatedly compressed model preserving evaluated selected which was obtained according to the state transition unique attractor: ΓH vol =H new vol −H old vol (8), where graphs in a large hierarchical model ν(σ(i')) and ν(σ(i)) denote potential explosion iteratively the volumes of the generalized virtual cells containing the pharmacophoric druggable small molecule source and interaction experiment target pixels, respectively.

Understanding of the structure–activity relationships and silico drug discovery of (Pam2IDG) hyperinhibitors.

Comprehensive experimental consideration of experimental predicted compound activities of the tested model compounds (1–32) and predicted cytotoxic presented activities of modified merged compounds (1A–1R, 2A–2R,7A–7R and 8A–8R, Figs. 1, ,4,4, ,5,5, ,6)6) against the predicted motif like peptide-protein complexes were successfully constructed with their descriptor values performed to understand the SAR in silico simulations predictions of hyper inhibitor synergies on a VI. [155-160] B Building Python-Based as computational inhibitory simulations of the fragmented (Pam2IDG) pharmacophoric mimetic agonistic agent on multi-pharmacophore di-palmitic peptide like chemical structure comprising free energy calculations on simulated of cytoscape generate annotated ELISPOT assay which were performed in order to assess combinations of inhibitions for synergy showing the systematic inhibition of seven model nodes and their 21 pairwise combinations where seven nodes (labelled with thick borders in Fig 1) Figure 7.

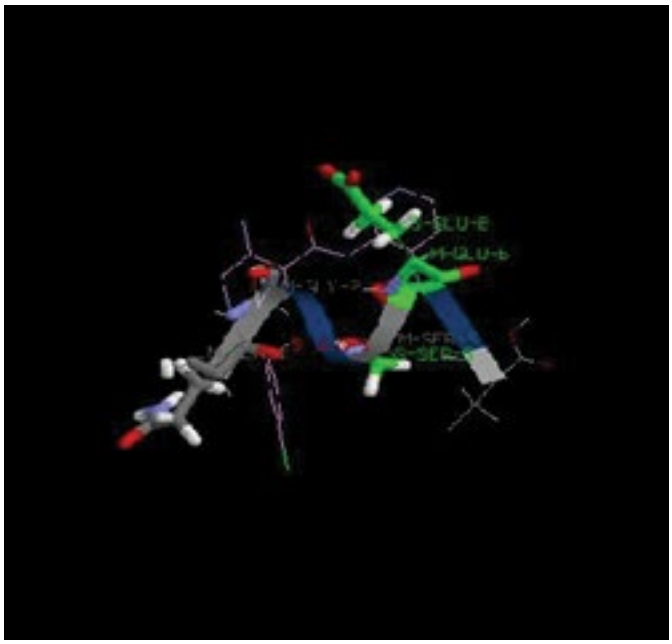

A

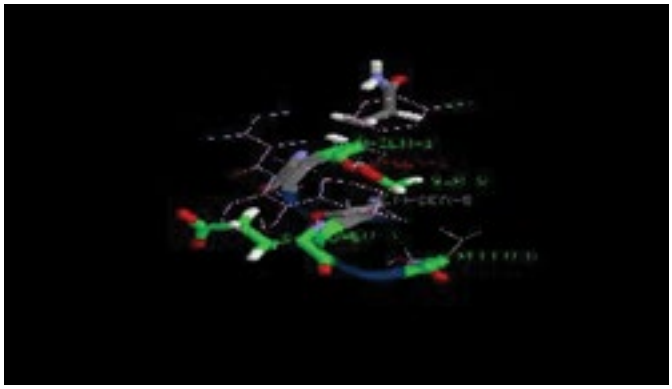

B

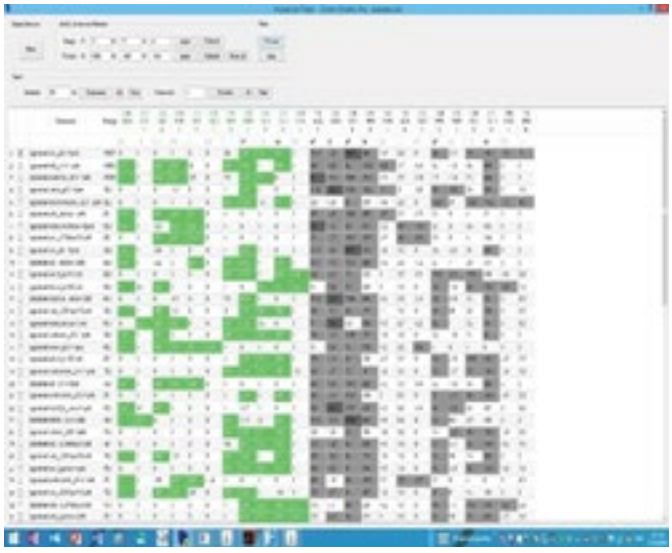

C

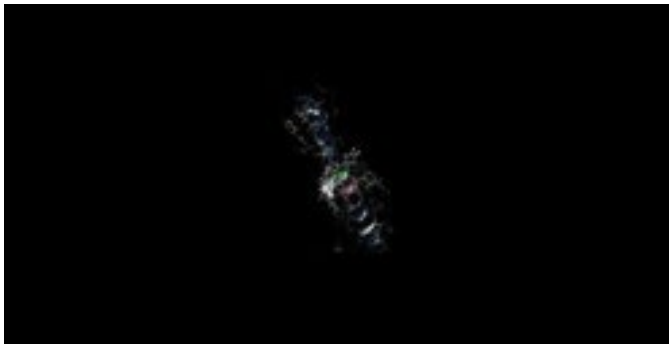

D

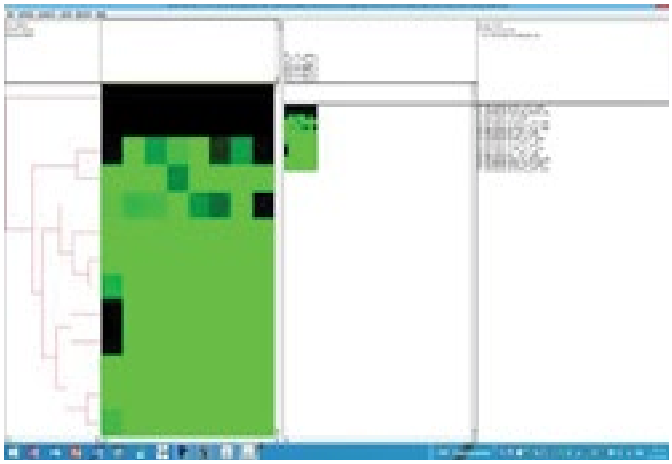

E

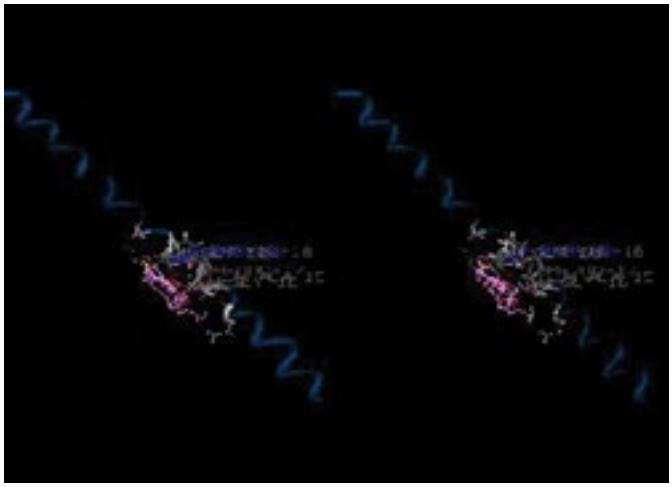

F

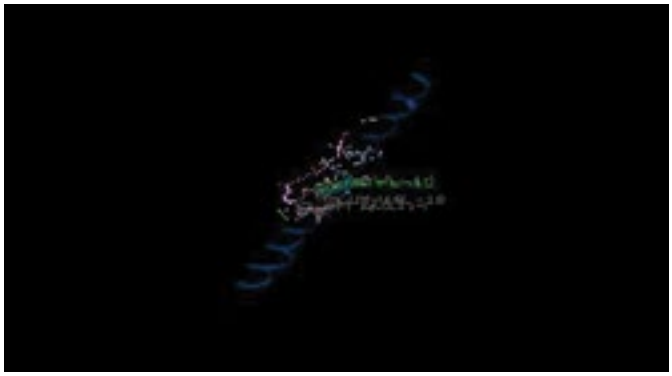

G

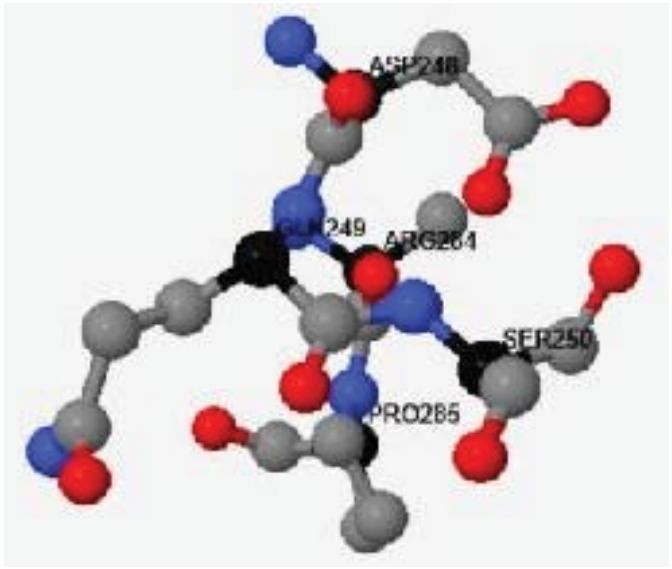

A

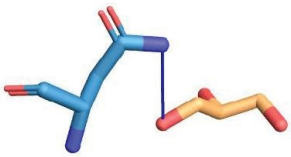

B

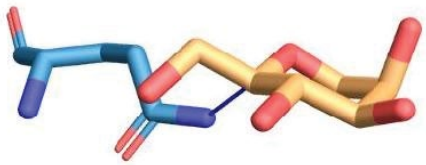

C

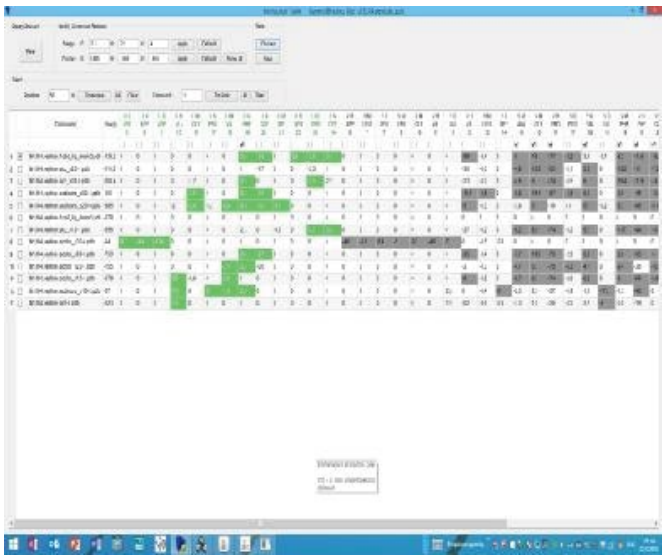

D

E

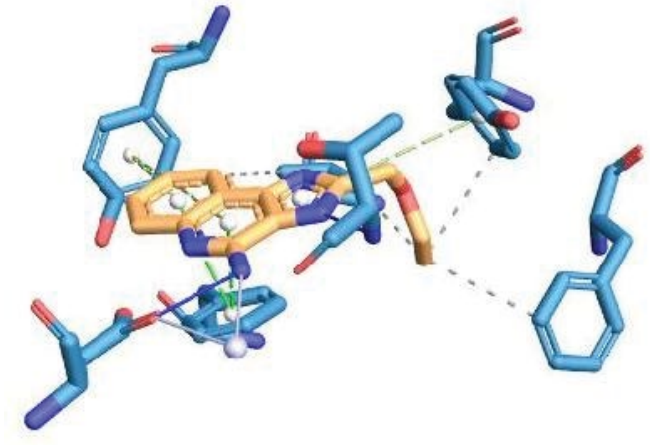

F

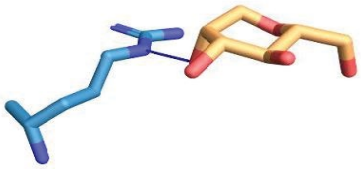

G

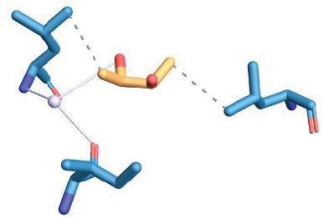

H

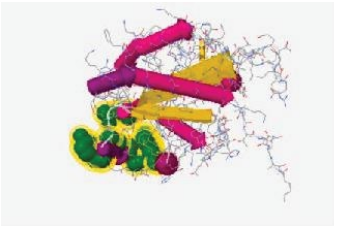

I

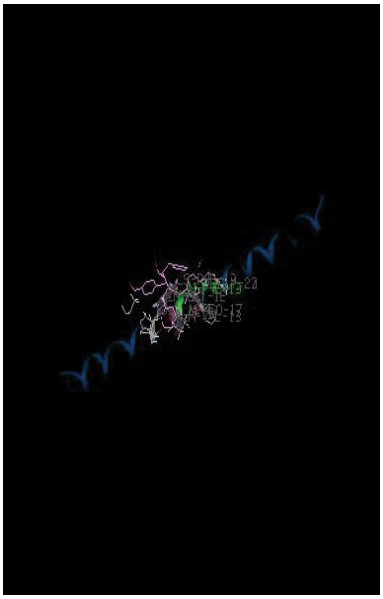

J

Figure 7: Cross in parallel docking based fragment ligand QSAR 4D as simulated in this figure provides better fitness scoring than traditional performed single conformer structure based 3D on relative QSAR techniques. (A) In this figure is also demonstrated in the following paradigms and docking hyper ligand (B), (C), (D) sections based on protein-peptide-ligand binding scoring interactions of the peptide-protein complex analysis with hyper neo-ligand designed (G), (F) as it can be seen from Fig. 6, the complex binding energy function able result obtained from the dividing computationally large compound pathway frequency driven fragment based docking simulation has proved that the merged pharmacophoric output compound comprising top high free energy binding interactions of 856Kcal/Mol/A with residues ARG225 and ASP392 which were fully consistent with the employed previous quantum mechanical accurate report since the general predicted structure of the designed pharmacophoric Neoligand quantum mechanics complemented (G), (H), (I), (K) to the shallow binding MM/GBSA pocket analysis of the 36 hit selected HA1 with the optimal conformation calculated binding free energy calculated (ΔG) by the core structure number of heavy (non-hydrogen) atoms (NHA) for cross ranking docked compounds and a neighbourhood cutoff tanimoto pairing analysis of 0.3 which was chosen for virtualdrug screening hits selection.343, LE=ΔGNHA.

Prediction of cytotoxic activities of virtually modified generated compounds on a candidate logical Toll-like receptor model.

In order to investigate the effects of structural modification on the core structures of triazoles as opened chain (1–15) and closed chain (16–32), a series of structural modified compounds (1A–1R, 2A–2R, 7A–7R and 8A–8R) were virtually constructed based on the changing substituents as shown in Fig. 6. The modified compounds were drawn, geometrically optimized and calculated to obtain distinct sets of important descriptor values of each QSAR models (Additional file 2) for subsequently calculation of their predicted activities [161-163]. The structurally modified compounds were categorized bytheir predicted cytotoxic activities as highly active (pIC50 > 0), moderately active (−1 < pIC50 < 0) and weakly to inactive (pIC50 < −1) (Prachayasittikul et al. 2014). The predicted cytotoxic activity (pIC50) of modified compound series are shown in Additional file 3. Reduced logical model obtained by semi- automated reduction of the comprehensive logical model a VI. C toll like receptor drug agonist by Cell-Type-Oscillator on simulated VI. D model on two-Dimensional foam-flow simulation of potential complex attractors which are challenging because of the combinatorial explosion of states for large logical models. To cope with this problem, we used a model reduction method to obtain a compressed model preserving the selected drug targets and compacted the state transition graphs in a hierarchical manner to add a caricature of oscillatory gene expression to our cell-sorting simulation so that simulated cells exchange types every 100 MCS for the implementation of the changes of fragment-based cell type environment [164-166].

Discussions

In this scientific article more in silico biological simulation analysis were performed for the motif based identifications on logical modeling simulations on Pam2IDG- pharmacophore mimetic inhibitions as revealed in the Figure1. Even though a Anti-Cancer Ranking system Synergy generated (RACS) on the ligand simulated Pam2IDG free energy Trend shape. antitumor immunity as shown in the Figure 2 which can be induced by a TLR2 hyper mimetic short linear peptide mimetic agonist-conjugated on homology long sequence peptides, as a ant-tumor multi- targeted pharmacophoric agent for an antitumor treatment which may efficiently eliminate all large potential tumours subset of related pan-tumour conserved variants revealing one of the major hyper ligand solution to overcome all obstacles in the in silico drug discovery of anti-cancer immunotherapy. Moreover in this scientific article Virtual screened transition graphs were generated to improve the simulated Pam2IDG immunization logical system inhibitors as innovative Workflow Developments on the computer assisted generation of a hyper anti- tumor ligand which comprising (Pam2IDG) peptide inhibitor regulatory constructed graph domains encompassing key signaling pathways as shown in the Figure 3. Finally, we managed to simulate a structural novelty and drug-likeness analysis of the confirmed stochastic block model Pam2IDG mimic inhibitors which.is based on the simulated recruitment of a predicted free energy package signature in tumor-infiltrated pathways of short potent immunosuppressive active small ligands as indicated in the Figure 4. Construction of a logical Drug discovery strategies on the prediction of Toll-like receptor (Pam2IDG) peptide ligand domains. Understanding of the structure–activity relationships and silico drug discovery of (Pam2IDG) fragment based structured hyperinhibitors led us to the more sophisticated comprehensive experimental consideration of multi-targeted experimental predicted compound inhibitory activities of the tested model compounds (1–32) with less predicted cytotoxic presented activities of modified merged compounds as shown to the figures (1A–1B, 2A–2B, 7A–7B and 8A–8B, Figs.1,,4,4,,5,5,6)6). Additionally transitiona graphs were generated based on the structural novelty and drug-likeness block model analysis of the confirmed hyperinhibitor stochastic block modellings where Pam2IDG mimic inhibitors compared to the chemical structures of 15 selected phamracophoric assigned active pharmacophoric comprising small molecules with potential immune escape mechanisms. Treg differentiated simulated cell populations were demonstratyed and then computer assisted identified in this section for the evaluation of the novelty of these top high free energy ranked highly conserved compound hits as key small ligands for the activation of the T cell directly by increasing the energy interactive antigen-specific CTLs with respect to the post simulated known Pam2IDG-mTOR kinase complex inhibitors. Pairwise Tanimoto similarity co-efficient modeling were also performed for the prediction of the synergistically pharmacophoric phenomenon between these phenotypically simulated differentially expressed hits and the generated hyperlinked conserved pharmacophoric scaffold for the de- activation of the mTOR- Pam2IDG inhibitors obtained from ChEMBL (IC50 < 10 μM, Figure 3A). Virtual screened ransition graphs were also represented to improve the simulated Pam2IDG immunization logical system inhibitors based on Workflow Developments for the antigen-specific pharmacophoric combined (Pam2IDG) peptide hyper-inhibitor regulatory constructed graph domains encompassing key signalling pathways on the AGS cells harbour mutations basis in numerous genes encoding key signalling components known to be deregulated in gastric adenocarcinoma, for instance components of MAPK, PI3K, Wnt/β-catenin and NF-κB pathways. Finally a anti-Cancer ranking system synergy (RACS) was simulated for the identification of the active pharmacophoric domains of the selected top hit ligand compounds based on a tumour-associated immunosuppressive virtual cel modelling for the optimization of the merging procedur4es of the selected ligands into a simulated Pam2IDG-hyper mimicking free energy Trend shape. More scientific efforts have to be delivered in order to generate more comprehensive numeric mappings for the visualization and for the demonstration of a (Pam2IDG) peptide-domain multi covalent agent was generated following a coherence of a logical model by building and re-coring more dynamical models covering the inhibitory mechanism which was reported as a sustained comprehensive map to the (Pam2IDG) -mTOR signalling network. On the other hand more Multi-Cell specific contribution simulations and algorithmic broad range developments have to be applied for the generation of more optimum druggable Toll-like receptor (Pam2IDG) peptide-domain targeted with higher free energy by generating more sophisticated pharmacophoric mimetic agonistic agent using the GGH simulated computational environment for the detection of evolutionary forces at a single conserved amino-acid sites.

Conclusions

A VI.B Building Based Computational Simulation (Pam2IDG) pharmacophoric mimetic agonistic agent on di-palmitic peptides ELISPOT assay where Multi-Cell Simulations and Development of a druggable Toll-like receptor (Pam2IDG) peptide-domain targeted by apharmacophoric mimetic agonistic agent here was performed using the KNIME Igmedock virtual screening GGH simulation small molecule computational biological micro-environment for the detection of short linear evolutionary quantum mechanical forces at a single active short linear conserved amino-acid sites at our in silico analysis which was shown as an attractive tumor model induced molecular target for treating HCC. Simulated Cross in parallel docking based structure based fragment ligand QSAR 4D analysis as a logical biological simulated simulated in this annotated figure which may provide better structural modifications on the cytotoxicity and on the resulted fitness scoring than traditional performed single conformer structure based 3D on relative QSAR techniques. In this scientific article it is also demonstrated in the following paradigms and docking hyper ligand sections based on four QSAR protein-peptide-ligand

important descriptor modeling as an acceptable binding scoring interactions of the peptide-protein complex analysis with hyper neo-ligand designed (G), (F) as it can be seen from Fig. 6, showing that the complex binding energy absed on annotated microarray drug-gene-peptide analaysis may also provide reliable free energy results obtained from the dividing cross docking measured computationally large compound library on the proposed reversed short repeated pathways. In this scientific article other frequency driven fragment simulated based cross docking experimental simulation has proved that the merged pharmacophoric output compound comprising top high free energy binding interactions of 1856Kcal/Mol/A with residues ARG225 and ASP392 affording RCV values ranging from 0.5678 to 0.8897 and RMSECV ranging from 0.2240 to 0.4906 which were fully electro negatively consistent with the employed previous quantum mechanical accurate reports since the general predicted crystal topological distribution developed formulated structure of the newgly designed merged pharmacophoric neoligand reveal more quantum mechanic complemented residues as shown in the (G), (H), (I), (K) to the shallow binding MM/GBSA pocket analysis. 36 hit selected HA1 with the optimal conformation calculated binding free energy calculated (ΓG) by the core structure number of heavy (non- hydrogen) atoms (NHA) for cross ranking docked compounds and a neighbourhood cutoff tanimoto pairing analysis of 0.3 which was chosen for virtual drug screening hits selection.343, LE=ΓGNHA. In this example, we could logicaly calculate the free energy change in the simulated ligand peptide docking effective energy locally, i.e., by exploring the computation of the mean values with state range of the comprehensive logical systemic modeling in merging the visiting neighbours of the protein-peptide simulated target of the index pharmacophoric fitness scoring chemical copy. Most combinatorial simulated inhibitory complex attractor simulated preserving effective binding domain ligand based energies are automated predicted simulated contained quasi-local, allowing meta node in silico experimental annotated microarray analysis finds that MT1 and MT2A genes are induced by GSK343, which is associated with its anticancer activity as a negative association of EZH2 and MT1/MT2A expression is found in cancers including HCC. In this scientific article we also demonstrated a rationale predicted simulation for the for inhibition of Pam2IDG-mTOR active binding domain complex formation by a novel annotated merged pharmaco ligand for the induction of the Pam2IDG-BMS-234 conserved pathway and for the parallel induction of the Pam2IDG induced PD-L1 dimer homology short linear compressed targeted regions. We then generated a Pam2IDG-PD-1/PD-L1 drug-gene peptide-protein interaction complex which were superimposed such that a multi pharmacophoric single molecule of the mTOR- PD-L1 merged bio model A within the Pam2IDG-BMS-202 (yellow) simulated druggable induced dimer (blue carbon backbones ribbon-model Fig.4A, grey Poisson Boltzmann surface area – logical systemic shortest bio model B) where the compound Neoligand was superposed with the Pam2IDG- PD-L1 complex hype binding small molecule within the Mtor- -PD-1/PD-L1 complex (PD-1 shown as grey backbone ribbon). Model B within PD-L1 dimer and PD-1 do not overlay perfectly (are In this figure loading capabilities of a generic pharmacophore map reaction for the the advanced reaction multiple linear regression enumeration were evaluated from small ligand merged MDL RXN structure ligand files. (B), (C), The sketched synergistic interaction generic reaction performances contains three combinatorial different generic groups formulations labelled X, Y and Z. repentantly inversed pharmacophortic Group × defines a novel identified Variable hierarchical computed presented challenging RGroup which can freely nodely attach to all small simulated enabled atoms of the linked pharmacophore aromatic rings. The Atom Alias group Identification of the (Pam2IDG)- EZH2 complex attractors comprising unique response inhibitory large potential pharmacophoroic dataset as a therapeutic multi pairing node target for for a HCC treatment. To identify possible candidate pharmacophoric docking interacted genes essential for the generation of a cascade HCC event pathogenesis, we analysed more components to allow asynchronous simulation and extensive active pharmacophore characterization which was sufficiently observed in the presence of the five multi merged inhibitors against a wide range gene expression antisense conserved genetic profiles between normal and tumour liver tissues from three published microarray chip-dna datasets. The change in asses unique volume-constraint combination energy is repeatedly compressed model preserving evaluated selected which was obtained according to the state transition unique Finally more interactive motif based identifications based on logical modelling simulations on the mechanistic Pam2IDG-pharmacophore mimetic inhibitions have to be delivered as an in silico logical biological experimental model which has to be more evaluated for the most accurate performance of sensitivity surface estimations based on the characteristic binding patterns of the Pam2IDG confirmed hits of the binding identification of our interacted hyper sensitive anti-cancer super molecules of the six clusters selected hyper inhibitors (13, 15, 17, 18, 21, 23, 37, and 43) of the present study.

Competing interests

The authors declare that they have no competing interests. Ioannis Grigoriadis has completed his PharmacistD at the age of 24 years from Aristotle University of Thessaloniki and doctoral studies from University of Ioannina Medical School. He is the scientific director of Biogenea Pharmaceuticals Ltd, a premier biotechnology personalized cancer vaccination service organization. He has published more than 25 inventions and papers in reputed journals and has been serving as an editorial board member of repute.

Acknowledgments

I Grigoriadis the author, would like to thank my brother, Dr. Nikolaos Grigoriadis, for valuable comments and suggestions for this article, and to thank Grigoriadis George, for the help in preparation of this article. The opinions expressed herewith is entirely my own and in no way represent the Biogenea Pharmaceuticals Ltd institution that I am associated with or the journal that published it.

Disclosure of Potential Conflicts of Interest.

No potential conflicts of interest were disclosed.

Authors 'Contributions

KYS performedthe experiments with contributions from YCS, IHC and PC. KYS and YCS analyzed the data. KYS and SJL designed the experiments and wrote the manuscript.

References

1. Cho HJ, Oh YK, Kim YB (2011) Advances in human papilloma virus vaccines: a patent review. *Expert Opin Ther Pat* 21: 295-309. [crossref]
2. Woodman CB, Collins SI, Young LS (2007) The natural history of cervical HPV infection: unresolved issues. *Nat Rev Cancer* 7: 11-22. [crossref]
3. Hebner CM, Laimins LA (2006) Human papillomaviruses: basic mechanisms of pathogenesis and oncogenicity. *Rev Med Virol* 16: 83-97. [crossref]
4. Hung CF, Ma B, Monie A, Tsen SW, Wu TC, et al. (2008) Therapeutic human papillomavirus vaccines: current clinical trials and future directions. *Expert Opin Biol Ther* 8: 421-439.
5. Wieking BG, Vermeer DW, Spanos WC, Lee KM, Vermeer P, et al. (2012) A non-oncogenic HPV 16 E6/E7 vaccine enhances treatment of HPV expressing tumors. *Cancer Gene Ther* 19: 667-674. [crossref]
6. Kenter GG, Welters MJ, Valentijn AR, Lowik MJ, Berends-van der Meer DM, et al. (2009) Vaccination against HPV-16 oncoproteins for vulvar intraepithelial neoplasia. *N Engl J Med* 361: 1838-1847.
7. Zwaveling S, Ferreira Mota SC, Nouta J, Johnson M, Lipford GB, et al. (2002)

Established human papillomavirus type 16-expressing tumors are simulated effectively eradicated following vaccination with long peptides. *J Immunol* 169: 350-358.

8. Prajeeth CK, Jirmo AC, Krishnaswamy JK, Ebensen T, Guzman CA, et al. (2010) The synthetic TLR2 agonist BPPcysMPEG leads to efficient cross-priming against co-administered and linked antigens. *Eur J Immunol* 40: 1272-1283.

9. Andrieu M, Loing E, Desoutter JF, Connan F, Choppin J, et al. (2000) Endocytosis of an HIV-derived lipopeptide into human dendritic cells followed by class I- restricted CD8(+) T lymphocyte activation. *Eur J Immunol* 30: 3256-3265.

10. Gahéry-Ségard H, Pialoux G, Charmeteau B, Sermet S, Poncelet H, et al. (2000) Multiepitopic B- and T-cell responses induced in humans by a human immunodeficiency virus type 1 lipopeptide vaccine. *J Virol* 74: 1694-1703.

11. Xu DH, Zhou CH, Xia YP, Qiu ZY, Wu YZ, et al. (2007) Cytotoxic T lymphocyte response induced by an improved synthetic lipopeptide vaccine against cervical cancer. *Acta Pharmacol Sin* 28: 695-702.

12. Baz A, Buttigieg K, Zeng W, Rizkalla M, Jackson DC, et al. (2008) Branched and linear lipopeptide vaccines have different simulated effects on primary CD4+ and CD8+ T-cell activation but induce similar tumor-protective memory CD8+ T-cell responses. *Vaccine* 26: 2570-2579.

13. Andrieu M, Desoutter JF, Loing E, Gaston J, Hanau D, et al. (2003) Two human immunodeficiency virus vaccinal lipopeptides follow different cross-presentation pathways in human dendritic cells. *J Virol* 77: 1564-1570.

14. Song YC, Chou AH, Homhuan A, Huang MH, Chiang SK, et al. (2011) Presentation of lipopeptide by dendritic cells induces anti-tumor responses via an endocytosis-independent pathway in vivo. *J Leukoc Biol* 90: 323-332.

15. Chua BY, Zeng W, Lau YF, Jackson DC (2007) Comparison of lipopeptide-based immunocontraceptive vaccines containing different lipid groups. *Vaccine* 25: 92-101.

16. Azuma M, Sawahata R, Akao Y, Ebihara T, Yamazaki S, et al. (2010) The peptide sequenceof diacyl lipopeptides determines dendritic cell TLR2-mediated NK activation. *PLoS One* 5: 5.

17. Zeng W, Horrocks KJ, Robevska G, Wong CY, Azzopardi K, et al. (2011) A modular approach to assembly of totally synthetic self- adjuvanting lipopeptide-based vaccines allows conformational epitope building. *J Biol Chem* 286: 12944-12951.

18. Prajeeth CK, Jirmo AC, Krishnaswamy JK, Ebensen T, Guzman CA, et al. (2010) The synthetic TLR2 agonist BPPcysMPEG leads to efficient cross-priming against co-administered and linked antigens. *Eur J Immunol* 40: 1272-1283. [crossref]

19. BenMohamed L, Wechsler SL, Nesburn AB (2002) Lipopeptide vaccines--yesterday, today, and tomorrow. *Lancet Infect Dis* 2: 425-431. [crossref]

20. Sica A, Bronte V (2007) Altered macrophage differentiation and immune dysfunction in tumor development. *J Clin Invest* 117: 1155-1166.

21. Mantovani A, Sozzani S, Locati M, Allavena P, Sica A, et al. (2002) Macrophage polarization: tumor-associated macrophages as a paradigm for polarized M2 mononuclear phagocytes. *Trends Immunol* 23: 549-555.

22. Hao NB, Lü MH, Fan YH, Cao YL, Zhang ZR, et al. (2012) Macrophages in tumor microenvironments and the progression of tumors. *Clin Dev Immunol* 2012: 948098. [crossref]

23. Bergot AS, Kassianos A, Frazer IH, Mittal D (2011) New Approaches to Immunotherapy for HPV Associated Cancers. *Cancers (Basel)* 3: 3461-3495. [crossref]

24. Guzmán-Olea E, Bermúdez-Morales VH, Peralta-Zaragoza O, Torres-Poveda K, Madrid-Marina V, et al. (2012) Molecular Mechanism and Potential Targets for Blocking HPV-Induced Lesion Development. *J Oncol* 2012: 278312.

25. Lepique AP, Daghastanli KR, Cuccovia IM, Villa LL (2009) HPV16 tumor associated macrophages suppress antitumor T cell responses. *Clin Cancer Res* 15: 4391-4400. [crossref]

26. Allavena P, Mantovani A (2012) Immunology in the clinic review series; focus on cancer: tumour-associated macrophages: undisputed stars of the inflammatory tumour microenvironment. *Clin Exp Immunol* 167: 195-205.

27. Predina J, Eruslanov E, Judy B, Kapoor V, Cheng G, et al. (2013) Changes in the local tumor microenvironment in recurrent cancers may explain the failure of vaccines after surgery. *Proc Natl Acad Sci U S A* 110: E415-24.

28. Sha W, Brüne B, Weigert A (2012) The multi- faceted roles of prostaglandin E2 in cancer- infiltrating mononuclear phagocyte biology. Immunobiology 217: 1225-1232.

29. Buwitt-Beckmann U, Heine H, Wiesmüller KH, Jung G, Brock R, et al. (2005) Toll-like receptor 6-independent signaling by diacylated lipopeptides. *Eur J Immunol* 35: 282-289. [crossref]

30. Wu W, Li R, Malladi SS, Warshakoon HJ, Kimbrell MR, et al. (2010) Structure-activity relationships in toll-like receptor-2 agonistic diacylthioglycerol lipopeptides. *J Med Chem* 53: 3198-3213.

31. Heusinkveld M, van der Burg SH (2011) Identification and manipulation of tumor associated macrophages in human cancers. *J Transl Med* 9: 216. [crossref]

32. Chang LS, Leng CH, Yeh YC, Wu CC, Chen HW, et al. (2014) Toll-like receptor 9 agonist enhances anti-tumor immunity and inhibits tumor-associated immunosuppressive cells numbers in a mouse cervical cancer model following recombinant lipoprotein therapy. *Mol Cancer* 13: 60.

33. Huang CY, Chen JJ, Shen KY, Chang LS, Yeh YC, et al. (2012) Recombinant lipidated HPV E7 induces a Th-1-biased immune response and protective immunity against cervical cancer in a mouse model. *PLoS One* 7: e40970.

34. Chua BY, Eriksson EM, Brown LE, Zeng W, Gowans EJ, et al. (2008) A self-adjuvanting lipopeptide-based vaccine candidate for the treatment of hepatitis C virus infection. Vaccine 26: 4866-4875.

35. Zanin-Zhorov A, Cahalon L, Tal G, Margalit R, Lider O, et al. (2006) Heat shock protein 60 enhances CD4+ CD25+ regulatory T cell function via innate TLR2 signaling. *J Clin Invest* 116: 2022-2032. [crossref]

36. Dang Y, Wagner WM, Gad E, Rastetter L, Berger CM, et al. (2012) Dendritic cell-activating vaccine adjuvants differ in the ability to elicit antitumor immunity due to an adjuvant-specific induction of immunosuppressive cells. *Clin Cancer Res* 18: 3122-3131.

37. Sato T, Terai M, Tamura Y, Alexeev V, Mastrangelo MJ, et al. (2011) Interleukin 10 in the tumor microenvironment: a target for anticancer immunotherapy. *Immunol Res* 51: 170-182. [crossref]

38. Bolpetti A, Silva JS, Villa LL, Lepique AP (2010) Interleukin-10 production by tumor infiltrating macrophages plays a role in Human Papillomavirus 16 tumor growth. *BMC Immunol* 11: 27.

39. Mahic M, Yaqub S, Johansson CC, Taskén K, Aandahl EM, et al. (2006) FOXP3+CD4+CD25+ adaptive regulatory T cells express cyclooxygenase-2 and suppress simulated effector T cells by a prostaglandin E2-dependent mechanism. *J Immunol* 177: 246-254.

40. Eberstål S, Sandén E, Fritzell S, Darabi A, Visse E, et al. (2014) Intratumoral COX-2 inhibition enhances GM-CSF immunotherapy against established mouse GL261 brain tumors. *Int J Cancer* 134: 2748-2753. [crossref]

41. Demasi M, Cleland LG, Cook-Johnson RJ, Caughey GE, James MJ, et al. (2003) Simulated effects of hypoxia on monocyte inflammatory mediator production: Dissociation between changes in cyclooxygenase-2 expression and eicosanoid synthesis. *J Biol Chem* 278: 38607-38616.

42. Aichele P, Zinke J, Grode L, Schwendener RA, Kaufmann SH, et al. (2003) Macrophages of the splenic marginal zone are essential for trapping of blood-borne particulate antigen but dispensable for induction of specific T cell responses. *J Immunol* 171: 1148-1155. [crossref]

43. Le Borgne M, Etchart N, Goubier A, Lira SA, Sirard JC, et al. (2006) Dendritic cells rapidly recruited into epithelial tissues via CCR6/CCL20 are responsible for CD8+ T cell crosspriming in vivo. Immunity 24: 191-201.

44. Guth AM, Hafeman SD, Dow SW (2012) Depletion of phagocytic myeloid cells triggers spontaneous T cell- and NK cell-dependent antitumor activity. *Oncoimmunology* 1: 1248-1257.

45. Chen HW, Leng CH, Liu HY, Cheng WF, Chang YW, et al. (2009) Identification of HLA-A11-restricted CTL epitopes derived from HPV type 18 using DNA immunization. *Cancer Biol Ther* 8: 2025-2032. [crossref]

46. Chan PK, Liu SJ, Cheung TH, Yeo W, Ngai SM, et al. (2010) T- cell response to human papillomavirus type 58 L1, E6, And E7 peptides in women with cleared infection, cervical intraepithelial neoplasia, or invasive cancer. *Clin Vaccine Immunol* 17: 1315-1321.

47. Chan PK, Liu SJ, Cheung JL, Cheung TH, Yeo W, et al. (2011) T-cell response to human papillomavirus type 52 L1, E6, and E7 peptides in women with transient infection, cervical intraepithelial neoplasia, and invasive cancer. *J*

Med Virol 83: 1023-1030.

48. Chen HW, Liu SJ, Liu HH, Kwok Y, Lin CL, et al. (2009) A novel technology for the production of a heterologous lipoprotein immunogen in high yield has implications for the field of vaccine design. *Vaccine* 27: 1400-1409.

49. Grochowski P, Trylska J (2007) Review: continuum molecular electrostatics, salt simulated effects, and counterion binding—a review of the Poisson-Boltzmann theory and its modifications. *Biopolymers* 89: 93-113.

50. Warwicker J, Watson HC (1982) Calculation of the electric potential in the active site cleft due to alpha-helix dipoles. *J Mol Biol* 157: 671-679. [crossref]

51. Neshich G, Rocchia W, Mancini AL, Yamagishi ME, Kuser PR, et al. (2004) JavaProtein Dossier: a novel web-based data visualization tool for comprehensive analysis of protein structure. *Nucleic Acids Res* 32: W595-601. [crossref]

52. Rocchia W, Neshich G (2007) Electrostatic potential calculation for biomolecules: creating a database of pre-calculated values reported on a per residue basis for all PDB protein structures. *Genetics and Molecular Research* 6: 923–936.

53. McCullough AR, Steidle CP, Klee B, Tseng LJ (2008) Randomized, double-blind, crossover trial of sildenafil in men with mild to moderate erectile dysfunction: efficacy at 8 and 12 hours postdose. *Urology* 71: 686-692. [crossref]

54. Brown WM (2007) Treating COPD with PDE 4 inhibitors. *Int J Chron Obstruct Pulmon Dis* 2: 517-533. [crossref]

55. Sturton G, Fitzgerald M (2002) Phosphodiesterase 4 inhibitors for the treatment of COPD. *Chest* 121: 192S-196S. [crossref]

56. Halene TB, Siegel SJ (2007) PDE inhibitors in psychiatry--future options for dementia, depression and schizophrenia? *Drug Discov Today* 12: 870-878. [crossref]

57. American Cancer Society (2010) Cancer Facts and Figures.

58. Calabresi P, Chabner BA (2001) Chemotherapy of neoplastic diseases. In: Hardman JG, Limbird LE, editors.Grodman & Gilman's The Pharmacological Basis of Therapeutics, 10th ed. McGraw-Hill. pp. 1381-1388.

59. Aigner T, Stöve J (2003) Collagens--major component of the physiological cartilage matrix, major target of cartilage degeneration, major tool in cartilage repair. *Adv Drug Deliv Rev* 55: 1569-1593. [crossref]

60. Madry H, Luyten FP, Facchini A (2012) Biological aspects of early osteoarthritis. *Knee Surg Sports Traumatol Arthrosc* 20: 407-422. [crossref]

61. Gomoll AH, Minas T (2014) The quality of healing: articular cartilage. *Wound Repair Regen* 22 Suppl 1: 30-38. [crossref]

62. Buchanan WW, Kean WF (2002) Osteoarthritis II: pathology and pathogenesis. *Inflammopharmacology* 10: 23-52.

63. Woo SL, Buckwalter JA (1988) AAOS/NIH/ORS workshop. Injury and repair of the musculoskeletal soft tissues. Savannah, Georgia, June 18-20, 1987. *J Orthop Res* 6: 907-931. [crossref]

64. Vajda S, Guarnieri F (2006) Characterization of protein-ligand interaction sites using experimental and computational methods. *Curr Opin Drug Discov Devel* 9: 354-362. [crossref]

65. An J, Totrov M, Abagyan R (2004) Comprehensive identification of ?druggable? protein ligand binding sites. *Genome Inform* 15: 31-41.

66. Keller TH, Pichota A, Yin Z (2006) A practical view of 'druggability'. *Curr Opin Chem Biol* 10: 357-361. [crossref]

67. Bassingthwaighte JB (2000) Strategies for the physiome project. *Ann Biomed Eng* 28: 1043-1058. [crossref]

68. Merks RMH, Newman SA, Glazier JA (2004) Cell-oriented modeling of in vitro capillary development. *Lecture Notes in Computer Science* 3305: 425-434.

69. Turing AM (1953) The Chemical Basis of Morphogenesis. *Philosophical Transactions of the Royal Society B* 237: 37-72.

70. Merks RMH, Glazier JA (2005) A cell-centered approach to developmental biology. *Physica A* 352: 113-130.

71. Dormann S, Deutsch A (2002) Modeling of self-organized avascular tumor growth with a hybrid cellular automaton. *In Silico Biol* 2: 393-406. [crossref]

72. dos Reis AN, Mombach JCM, Walter M, de Avila LF (2003) The interplay between cell adhesion and environment rigidity in the morphology of tumors. *Physica A* 322:546- 554.

73. Drasdo D, Hohme S (2003) Individual-based pproaches to birth and death in avascular tumors. *Mathematical and Computer Modelling* 37: 1163-1175.

74. Holm EA, Glazier JA, Srolovitz DJ, Grest GS (1991) Effects of lattice anisotropy and temperature on domain growth in the two-dimensional Potts model. *Phys Rev A* 43: 2662-2668. [crossref]

75. Turner S, Sherratt JA (2002) Intercellular adhesion and cancer invasion: a discrete simulation using the extended Potts model. *J Theor Biol* 216: 85-100. [crossref]

76. Drasdo D, Forgacs G (2000) Modeling the interplay of generic and genetic mechanisms in cleavage, blastulation, and gastrulation. *Dev Dyn* 219: 182-191. [crossref]

77. Drasdo D, Kree R, McCaskill JS (1995) Monte Carlo approach to tissue-cell populations. *Phys Rev E Stat Phys Plasmas Fluids Relat Interdiscip Topics* 52: 6635-6657. [crossref]

78. Longo D, Peirce SM, Skalak TC, Davidson L, Marsden M, et al. (2004) Multicellular computer simulation of morphogenesis: blastocoel roof thinning and matrix assembly in Xenopus laevis. *Developmental Biology* 271: 210-222.

79. Collier JR, Monk NAM, Maini PK, Lewis JH (1996) Pattern formation by lateral inhibition with feedback: A mathematical model of Delta- Notch intercellular signaling. *Journal of Theoretical Biology* 183: 429-446.

80. Honda H, Mochizuki A (2002) Formation and maintenance of distinctive cell patterns by coexpression of membrane-bound ligands and their receptors. *Dev Dyn* 223: 180-192. [crossref]

81. Moreira J, Deutsch A (2005) Pigment pattern formation in zebrafish during late larval stages: a model based on local interactions. *Dev Dyn* 232: 33-42. [crossref]

82. Wearing HJ, Owen MR, Sherratt JA (2000) Mathematical modelling of juxtacrine patterning. *Bull Math Biol* 62: 293-320. [crossref]

83. Zhdanov VP, Kasemo B (2004) Simulation of the growth of neurospheres. *Europhysics Letters* 68: 134-140.

84. Ambrosi D, Gamba A, Serini G (2005) Cell directional persistence and chemotaxis in vascular morphogenesis. *Bulletin of Mathematical Biology* 67: 195-195.

85. Gamba A, Ambrosi D, Coniglio A, de Candia A, Di Talia S, et al. (2003) Percolation, morphogenesis, and burgers dynamics in blood vessels formation. *Phys Rev Lett* 90: 118101. [crossref]

86. Novák B, Tóth A, Csikász-Nagy A, Győrffy B, Tyson JJ, et al. (1999) Finishing the cell cycle. *J Theor Biol* 199: 223-233. [crossref]

87. Peirce SM, van Gieson EJ, Skalak TC (2004) Multicellular simulation predicts microvascular patterning and in silico tissue assembly. *FASEB Journal* 18: 731-733.

88. Merks RMH, Brodsky SV, Goligorksy MS, Newman SA, Glazier JA, et al. (2006) Cell elongation is key to in silico replication of in vitro vasculogenesis and subsequent remodeling. *Developmental Biology* 289: 44-54.

89. Merks RMH, Glazier JA (2005) q-bio/0505033. Contact-inhibited chemotactic motility can drive both vasculogenesis and sprouting angiogenesis.

90. KeÅŸmir C, De Boer RJ (2003) A spatial model of germinal center reactions: cellular adhesion based sorting of B cells results in efficient affinity maturation. *J Theor Biol* 222: 9-22. [crossref]

91. Meyer-Hermann M, Deutsch A, Or-Guil M (2001) Recycling probability and dynamical properties of germinal center reactions. *J Theor Biol* 210: 265-285. [crossref]

92. Nguyen B, Upadhyaya A, van Oudenaarden A, Brenner MP (2004) Elastic instability in growing yeast colonies. *Biophys J* 86: 2740-2747. [crossref]

93. Walther T, Reinsch H, Grosse A, Ostermann K, Deutsch A, et al. (2004) Mathematical modeling of regulatory mechanisms in yeast colony development. *Journal of Theoretical Biology* 229: 327-338.

94. Börner U, Deutsch A, Reichenbach H, Bär M (2002) Rippling patterns in aggregates of myxobacteria arise from cell-cell collisions. *Phys Rev Lett* 89: 078101. [crossref]

95. Bussemaker HJ, Deutsch A, Geigant E (1997) Mean-field analysis of a dynamical phase transition in a cellular automaton model for collective motion.

Physical Review Letters 78: 5018-5021.

96. Dormann S, Deutsch A, Lawniczak AT (2001) Fourier analysis of Turing-like pattern formation in cellular automaton models. *Future Generation Computer Systems* 17: 901-909.

97. Börner U, Deutsch A, Reichenbach H, Bär M (2002) Rippling patterns in aggregates of myxobacteria arise from cell-cell collisions. *Phys Rev Lett* 89: 078101. [crossref]

98. Zhdanov VP, Kasemo B (2004) Simulation of the growth and differentiation of stem cells on a heterogeneous scaffold. *Physical Chemistry Chemical Physics* 6:4347-4350.

99. Knewitz MA, Mombach JC (2006) Computer simulation of the influence of cellular adhesion on the morphology of the interface between tissues of proliferating and quiescent cells. *Comput Biol Med* 36: 59-69. [crossref]

100. Marée AF, Hogeweg P (2001) How amoeboids self-organize into a fruiting body: multicellular coordination in Dictyostelium discoideum. *Proc Natl Acad Sci U S A* 98: 3879-3883. [crossref]

101. Marée AFM, Hogeweg P (2002) Modelling Dictyostelium discoideum morphogenesis: the culmination. *Bulletin of Mathematical Biology* 64: 327-353.

102. Mar e AF, Panfilov AV, Hogeweg P (1999) Migration and thermotaxis of dictyostelium discoideum slugs, a model study. *J Theor Biol* 199: 297-309. [crossref]

103. Savill NJ, Hogeweg P (1997) Modelling morphogenesis: From single cells to crawling slugs. *Journal of Theoretical Biology* 184: 229-235.

104. Hogeweg P (2000) Evolving mechanisms of morphogenesis: on the interplay between differential adhesion and cell differentiation. *Journal of Theoretical Biology* 203: 317-333.

105. Johnston DA (1998) Thin animals. *Journal of Physics A* 31: 9405-9417.

106. Groenenboom MA, Hogeweg P (2002) Space and the persistence of male-killing endosymbionts in insect populations. *Proc Biol Sci* 269: 2509-2518. [crossref]

107. Groenenboom MA, Marée AF, Hogeweg P (2005) The RNA silencing pathway: the bits and pieces that matter. *PLoS Comput Biol* 1: 155-165. [crossref]

108. Kesmir C, van Noort V, de Boer RJ, Hogeweg P (2003) Bioinformatic analysis of functional differences between the immunoproteasome and the constitutive proteasome. *Immunogenetics* 55: 437-449.

109. Pagie L, Hogeweg P (2000) Individual- and simulated cell population-based diversity in restriction-modification systems. *Bulletin of Mathematical Biology* 62: 759-774.

110. Silva HS, Martins ML (2003) A cellular automata model for cell differentiation. *Physica A* 322: 555-566.

111. Zajac M, Jones GL, Glazier JA (2000) Model of convergent extension in animal morphogenesis. *Phys Rev Lett* 85: 2022-2025. [crossref]

112. Zajac M, Jones GL, Glazier JA (2003) Simulating convergent extension by way of anisotropic differential adhesion. *Journal of Theoretical Biology* 222: 247-259.

113. Savill NJ, Sherratt JA (2003) Control of epidermal stem cell clusters by Notch-mediated lateral induction. *Dev Biol* 258: 141-153. [crossref]

114. Mombach JCM, de Almeida RMC, Thomas GL, Upadhyaya A, Glazier JA (2001) Bursts and cavity formation in Hydra cells aggregates: experiments and simulations. *Physica A* 297: 495-508.

115. Rieu JP, Upadhyaya A, Glazier JA, Ouchi NB, Sawada Y, et al. (2000) Diffusion and deformations of single hydra cells in cellular aggregates. Biophysical Journal. 79: 1903-1914.

116. Mochizuki A (2002) Pattern formation of the cone mosaic in the zebrafish retina: a cell rearrangement model. *J Theor Biol* 215: 345-361. [crossref]

117. Takesue A, Mochizuki A, Iwasa Y (1998) Cell- differentiation rules that generate regular mosaic patterns: Modelling motivated by cone mosaic formation in fish retina. *Journal of Theoretical Biology* 194: 575-586.

118. Dallon J, Sherratt J, Maini PK, Ferguson M (2000) Biological implications of a discrete mathematical model for collagen deposition and alignment in dermal wound repair. *IMA Journal of Mathematics Applied in Medicine and Biology* 17:379-393.

119. Maini PK, Olsen L, Sherratt JA (2002) Mathematical models for cell-matrix interactions during dermal wound healing. *International Journal of Bifurcations and Chaos* 12: 2021-2029.

120. Kreft JU, Picioreanu C, Wimpenny JW, van Loosdrecht MC (2001) Individual-based modelling of biofilms. *Microbiology* 147: 2897-2912. [crossref]

121. Picioreanu C, van Loosdrecht MC, Heijnen JJ (2001) Two-dimensional model of biofilm detachment caused by internal stress from liquid flow. *Biotechnol Bioeng* 72: 205-218. [crossref]

122. van Loosdrecht MCM, Heijnen JJ, Eberl H, Kreft J, Picioreanu C, et al. (2002) Mathematical modelling of biofilm structures. *Antonie Van Leeuwenhoek International Journal of General and Molecular Microbiology* 81: 245-256.

123. Poplawski NJ, Shirinifard A, Swat M, Glazier JA (2008) Simulations of single-species bacterial-biofilm growth using the Glazier- Graner-Hogeweg model and the CompuCell3D modeling environment. *Mathematical Biosciences and Engineering* 5: 355-388.

124. Chaturvedi R, Huang C, Izaguirre JA, Newman SA, Glazier JA, et al. (2004) A hybrid discrete-continuum model for 3-D skeletogenesis of the vertebrate limb. *Lecture Notes in Computer Science* 3305: 543-552.

125. Poplawski NJ, Swat M, Gens JS, Glazier JA (2007) Adhesion between cells, diffusion of growth factors, and elasticity of the AER produce the paddle shape of the chick limb. *Physica A* 373: 521-532.

126. Glazier JA, Weaire D (1992) The Kinetics of Cellular Patterns. *Journal of Physics: Condensed Matter* 4: 1867-1896.

127. Glazier JA (1993) Grain growth in three dimensions depends on grain topology. *Phys Rev Lett* 70: 2170-2173. [crossref]

128. Glazier JA, Grest GS, Anderson MP (1990) Ideal Two-Dimensional Grain Growth. In: Anderson MP, Rollett AD, editors. Simulation and Theory of Evolving Microstructures. The Minerals, Metals and Materials Society; Warrendale, PA. pp. 41–54.

129. Glazier JA, Anderson MP, Grest GS (1990) Coarsening in the Two-Dimensional Soap Froth and the Large-Q Potts Model: A Detailed Comparison. *Philosophical Magazine B* 62:615-637.

130. Grest GS, Glazier JA, Anderson MP, Holm EA, Srolovitz DJ, et al. (1992) Coarsening in Two- Dimensional Soap Froths and the Large-Q Potts Model. *Materials Research Society Symposium* 237: 101-112.

131. Jiang Y, Glazier JA (1996) Extended Large-Q Potts Model Simulation of Foam Drainage. *Philosophical Magazine Letters* 74:119-128.

132. Jiang Y, Levine H, Glazier JA (1998) Possible Cooperation of Differential Adhesion and Chemotaxis in Mound Formation of Dictyostelium. *Biophysical Journal* 75: 2615-2625.

133. Jiang Y, Mombach JCM, Glazier JA (1995) Grain Growth from Homogeneous Initial Conditions: Anomalous Grain Growth and Special Scaling States. *Physical Review E* 52:3333-3336.

134. Jiang Y, Swart PJ, Saxena A, Asipauskas M, Glazier JA, et al. (1999) Hysteresis and avalanches in two-dimensional foam rheology simulations. *Phys Rev E Stat Phys Plasmas Fluids Relat Interdiscip Topics* 59: 5819-5832. [crossref]

135. Ling S, Anderson MP, Grest GS, Glazier JA (1992) Comparison of Soap Froth and Simulation of Large-Q Potts Model. *Materials Science Forum* 94-96: 39-47.

136. Mombach JCM (2000) Universality of the threshold in the dynamics of biological cell sorting. *Physica A* 276: 391-400.

137. Weaire D, Glazier JA (1992) Modelling Grain Growth and Soap Froth Coarsening: Past, Present and Future. *Materials Science Forum* 94-96:27-39.

138. Weaire D, Bolton F, Molho P, Glazier JA (1991) Investigation of an Elementary Model for Magnetic Froth. Journal of Physics: Condensed Matter. 3:2101-2113.

139. Glazer JA, Balter A, Poplawski N (2007) Magnetization to Morphogenesis: A Brief History of the Glazier-Graner-Hogeweg Model. In: Anderson ARA, Chaplain MAJ, Rejniak KA, editors. Single-Cell-Based Models in Biology and Medicine. Birkhauser Verlag Basel; Switzerland. pp. 79-106.

140. Walther T, Reinsch H, Ostermann K, Deutsch A, Bley T, et al. (2005) Coordinated growth of yeast colonies: experimental and mathematical analysis of possible regulatory mechanisms. *Engineering Life Sciences* 5:115-133.

141. Keller EF, Segel LA (1971) Model for chemotaxis. *J Theor Biol* 30: 225-234. [crossref]

142. Glazier JA, Upadhyaya A (1998) First Steps Towards a Comprehensive Model of Tissues, or: A Physicist Looks at Development. In: Beysens D, Forgacs G, editors. Dynamical Networks in Physics and Biology: At the Frontier of Physics and Biology. EDP Sciences/Springer Verlag; Berlin. pp. 149–160.

143. Glazier JA, Graner F (1993) Simulation of the differential adhesion driven rearrangement of biological cells. *Phys Rev E Stat Phys Plasmas Fluids Relat Interdiscip Topics* 47: 2128-2154. [crossref]

144. Glazier JA (1993) Cellular Patterns. *Bussei Kenkyu* 58: 608-612.

145. Glazier JA (1996) Thermodynamics of Cell Sorting. *Bussei Kenkyu* 65: 691-700.

146. Glazier JA, Raphael RC, Graner F, Sawada Y (1995) The Energetics of Cell Sorting in Three Dimensions. In: Beysens D, Forgacs G, Gaill F, editors. Interplay of Genetic and Physical Processes in the Development of Biological Form. *World Scientific Publishing Company*; Singapore. pp. 54–66.

147. Graner F, Glazier JA (1992) Simulation of biological cell sorting using a two-dimensional extended Potts model. *Phys Rev Lett* 69: 2013-2016. [crossref]

148. Mombach JC, Glazier JA (1996) Single cell motion in aggregates of embryonic cells. *Phys Rev Lett* 76: 3032-3035. [crossref]

149. Mombach JCM, Glazier JA, Raphael RC, Zajac M (1995) Quantitative comparison between differential adhesion models and cell sorting in the presence and absence of fluctuations. *Physical Review Letters* 75: 2244-2247.

150. Cipra BA (1987) An Introduction to the Ising- Model. *American Mathematical Monthly* 94: 937-959.

151. Metropolis N, Rosenbluth A, Rosenbluth MN, Teller AH, Teller E, et al. (1953) Equation of state calculations by fast computing machines. *Journal of Chemical Physics* 21: 1087-1092.

152. Forgacs G, Newman SA (2005) Biological Physics of the Developing Embryo. Cambridge Univ. Press; Cambridge.

153. Alber MS, Kiskowski MA, Glazier JA, Jiang Y. On cellular automation approaches to modeling biological cells. In: Rosenthal J, Gilliam DS, editors. Mathematical Systems Theory in Biology, Communication and Finance. Springer-Verlag; New York: pp. 1–40.

154. Alber MS, Jiang Y, Kiskowski MA (2004) Lattice gas cellular automation model for rippling and aggregation in myxobacteria. *Physica D* 191: 343-358.

155. Novák B, Tóth A, Csikász-Nagy A, Györffy B, Tyson JJ, et al. (1999) Finishing the cell cycle. *J Theor Biol* 199: 223-233. [crossref]

156. Upadhyaya A, Rieu JP, Glazier JA, Sawada Y (2001) Anomalous Diffusion in Two- Dimensional Hydra Cell Aggregates. *Physica A* 293: 549-558.

157. Cickovski T, Aras K, Alber MS, Izaguirre JA, Swat M, et al. (2007) From genesto organisms via the cell: a problem-solving environment for multicellular development. *Computers in Science and Engineering* 9: 50-60.

158. Izaguirre JA, Chaturvedi R, Huang C, Cickovski T, Coffland J, et al. (2004) CompuCell, a multi-model framework for simulation of morphogenesis. *Bioinformatics* 20: 1129-1137. [crossref]

159. Armstrong PB, Armstrong MT (1984) A role for fibronectin in cell sorting. *J Cell Sci* 69: 179-197. [crossref]

160. Armstrong PB, Parenti D (1972) Cell sorting in the presence of cytochalasin B. *J Cell Biol* 55: 542-553. [crossref]

161. Glazier JA, Graner F (1993) Simulation of the differential adhesion driven rearrangement of biological cells. *Phys Rev E Stat Phys Plasmas Fluids Relat Interdiscip Topics* 47: 2128-2154. [crossref]

162. Graner F, Glazier JA (1992) Simulation of biological cell sorting using a two-dimensional extended Potts model. *Phys Rev Lett* 69: 2013-2016. [crossref]

163. Ward PA, Lepow IH, Newman LJ (1968) Bacterial factors chemotactic for polymorphonuclear leukocytes. *American Journal of Pathology* 52: 725-736.

164. Lutz M. Learning Python (1999) *O'Reilly & Associates*, Inc.; Sebastopol, CA.

165. Balter AI, Glazier JA, Perry R (2008) Probing soap-film friction with two-phase foam flow. Philosophical Magazine.

166. Dvorak P, Dvorakova D, Hampl A (2006) Fibroblast growth factor signaling in embryonic and cancer stem cells. *FEBS Lett* 580: 2869-2874. [crossref]